Nanoscale Horizons

ROYAL SOCIETY OF CHEMISTRY

MINIREVIEW

View Article Online
View Journal | View Issue

Cite this: *Nanoscale Horiz.*, 2025, **10**, 1932

Advancements in separator materials for aqueous zinc batteries

Qingshun Nian,†[a] Xinru Yang,†[a] Hu Hong,[a] Peng Chen,[a] Yuwei Zhao,[a] Haiming Lv[a] and Chunyi Zhi *[abcd]

Aqueous zinc (Zn) batteries (AZBs) are becoming promising candidates for grid-scale energy storage because of their inherent safety, cost-effectiveness, and high theoretical capacity. However, their widespread application is hindered by critical challenges, including Zn dendrite formation, hydrogen evolution reaction (HER), corrosion, and cathode material dissolution. The separator plays a crucial role in regulating ion transport, suppressing side reactions, and promoting uniform Zn deposition. While recent advancements in separator design have introduced various modification strategies to enhance electrochemical performance, a systematic classification based on the modification location remains lacking. This review provides a comprehensive analysis of recent advancements in AZB separators, categorized by modification position—anode side, cathode side, and full-separator modifications. Key modification strategies, including ion-selective layers, interfacial engineering, and composite functional membranes, are discussed in detail, with an emphasis on their effects on Zn^{2+} flux regulation, dendrite suppression, and long-term cycling stability. Additionally, emerging separator materials such as covalent organic frameworks (COFs), metal–organic frameworks (MOFs), and inorganic–organic hybrid separators are highlighted for their potential in optimizing battery performance. By elucidating the underlying mechanisms governing separator modifications, this review provides theoretical insights and design principles for the development of next-generation AZB separators. Finally, we discuss future research directions, focusing on separator thinness, enhanced ion selectivity, interface stability, corrosion resistance, and scalable manufacturing to accelerate the commercialization of high-performance AZBs.

Received 22nd March 2025,
Accepted 19th June 2025

DOI: 10.1039/d5nh00172b

rsc.li/nanoscale-horizons

1. Introduction

With the growing demand for sustainable energy storage, the development of safe, cost-effective, and high-performance battery technologies has become extremely important.[1–5] Although lithium-ion batteries (LIBs) have achieved widespread commercialization, their reliance on flammable organic electrolytes raises safety concerns.[6–17] Sodium-ion batteries (SIBs), which share similar electrochemical configurations with LIBs, also rely on organic electrolytes and thus suffer from comparable issues in terms of safety.[18–20] From the perspectives of safety, environmental sustainability, and resource abundance, aqueous batteries offer inherent advantages owing to their water-based electrolytes and the earth-abundant nature of water.

Compared with other aqueous battery systems—such as aqueous lithium-, sodium-, or potassium-ion batteries—AZBs benefit from the low redox potential and high theoretical capacity of the Zn metal anode, resulting in higher achievable energy density. Furthermore, in contrast to aqueous multivalent systems such as aluminum-ion batteries, AZBs exhibit better electrochemical reversibility.[21–31] AZBs have emerged as promising candidates for grid-scale energy storage due to their high safety, low cost, environmental friendliness, and high theoretical capacity (820 mAh g^{-1}; 5855 mAh cm^{-3}).[32–40] Despite these advantages, the practical use of AZBs is still limited by key challenges, including Zn dendrite growth, side reactions, and electrode corrosion.[41–46] Key strategies include electrode modification, electrolyte regulation, and separator optimization. Electrode modification focuses on constructing functional interface layers on the Zn anode surface or designing innovative electrode structures to regulate Zn deposition behavior, suppress side reactions, and improve electrode stability.[47–53] Coating a protective layer on the Zn anode surface can effectively suppress dendrite growth and side reactions. Common coating materials

[a] *Department of Materials Science and Engineering, City University of Hong Kong, Kowloon, Hong Kong SAR, 999077, China. E-mail: cy.zhi@cityu.edu.hk*
[b] *Hong Kong Institute for Advanced Study, City University of Hong Kong, Kowloon, Hong Kong SAR, 999077, China*
[c] *Hong Kong Institute for Clean Energy, City University of Hong Kong, Kowloon, Hong Kong SAR, 999077, China*
[d] *Centre for Advanced Nuclear Safety and Sustainable Development, City University of Hong Kong, Kowloon, Hong Kong SAR, 999077, China*
† These authors contributed equally to this work.

include carbon materials (such as reduced graphene oxide (rGO)[54] and carbon nanotubes (CNTs),[55] which have good conductivity and chemical stability, can distribute the electric field uniformly, and suppress dendrite growth),[56–58] metal oxides (such as ZnO,[59,60] CuO,[61] and In_2O_3,[62] which regulate Zn^{2+} flux and guide uniform Zn deposition), and polymers (such as PVDF-HFP[63] and PPPA,[64] which form flexible protective layers to suppress dendrite growth and corrosion). Alloys, such as Zn alloyed with other metals like Cu,[65] In,[66] Bi,[67] Sb,[68] and Sn,[69] can alter Zn's deposition potential and suppress dendrite growth and HER. In addition, the addition of small amounts of additives to the electrolyte can effectively suppress dendrite growth and side reactions. Common additives include metal ion additives (such as Ca^{2+},[70] Ga^{3+},[71] Y^{3+},[72] Ce^{3+},[73] which adsorb on the Zn surface to alter deposition behavior and suppress dendrite growth) and organic additives (such as PPGA[74] and DMSO,[75] which adsorb onto the Zn surface to regulate Zn deposition, mitigate corrosion, and lower water molecule activity to suppress the HER). Using high-concentration electrolytes can reduce the reactivity of water, suppress HER and side reactions, while enhancing the electrochemical window of the electrolyte.[76] In parallel, many reviews have focused on electrode modification and electrolyte optimization to improve Zn anode performance. However, the importance of separators has often been overlooked.

As an important but often overlooked component, the separator plays a key role in maintaining battery stability by physically separating the electrodes, optimizing ion transport, and reducing side reactions.[77] Recent advances in separator engineering have demonstrated significant potential in enhancing AZB cycling stability.[78–83] However, current separator modification strategies exhibit diversity and complexity, particularly with significant differences in the selection of modification locations—such as modifications on the anode side, cathode side, and full-separator modifications. Notably, existing reviews on AZB separators have not systematically summarized the research from the perspective of modification locations.

To address this gap, this review offers a detailed and organized analysis of advancements in AZB separators, categorized by modification position—anode side, cathode side, and full-separator modifications. By explaining the mechanisms of these modifications in controlling Zn^{2+} movement, suppressing dendrite growth, and reducing side reactions, this review aims to provide theoretical guidance and practical insights for designing high-performance AZB separators. Finally, it discusses future prospects for separator development, focusing on improving ion selectivity, structural stability, and scalable manufacturing to support the commercialization of AZBs.

2. Performance requirements and design guidelines for separators

Ideal separator materials for AZBs must meet several key performance criteria to ensure efficient and stable operation:

Cost ($<$\$1 per m^2): the cost should align with the low-cost positioning of AZBs and meet the economic requirements for grid-scale energy storage applications. Currently, the cost of commercial glass fiber (GF) separators is about \$0.5–0.8 per m^2, while the cost of new polymer separators still needs to be reduced further.

Electrical insulation: excellent electrical insulating properties are essential to prevent internal electron conduction in the battery, thus reducing the self-discharge rate (typically required to be $<$5% per month). Studies indicate that the volume resistivity of a high-quality separator should be greater than 10^9 Ω cm.

Porosity (40–70%) and pore size distribution: an ideal separator should have a uniform microporous structure (pore size 0.1–1 μm) to equalize ion flux distribution and suppress dendrite penetration. Excessively high porosity ($>$80%) may reduce mechanical strength, while excessively low porosity ($<$30%) can significantly increase ion transport resistance.

Electrolyte wettability: excellent wettability (contact angle $<30^\circ$) ensures high ionic conductivity. For example, surface-modified GF separators can achieve an ionic conductivity of 173 mS cm^{-1}, significantly outperforming traditional Celgard separators (around 0.3 mS cm^{-1}).

Mechanical strength: the wet-state tensile strength should exceed 5 MPa, and the puncture resistance should exceed 100 N to effectively resist penetration by Zn dendrites. Research shows that adding a nanofiber-reinforced layer can increase the mechanical strength of the separator by approximately 40%.

Thickness ($<$20 μm) and uniformity: ultra-thin and uniform separators can reduce the volume of inactive materials, thereby enhancing the energy density of the battery. Currently, advanced separators have a thickness controlled in the range of 10–15 μm, with thickness deviation less than ±2 μm.

Chemical stability: excellent chemical stability allows the separator to withstand the redox environment of the electrolyte (pH 3–14) without degradation. Experimental data shows that a high-quality separator should have a mass loss of less than 1% after being soaked in 1 M $ZnSO_4$ electrolyte for 30 days.

Thermal stability: a wide temperature tolerance range (−50 °C to 80 °C), with a low thermal shrinkage rate ($<$5%).

Environmental friendliness: the separator should be recyclable or biodegradable.

Processability: good processability and dimensional stability. These performance indicators are closely interconnected, and in practical applications, balancing them requires trade-offs tailored to specific usage scenarios. For example, increasing porosity can enhance ion conductivity but may reduce mechanical strength; increasing thickness can improve mechanical performance but will lower energy density. Therefore, separator design needs to seek the optimal balance between various performance parameters.

3. Structure and functional properties of common separators in AZBs

3.1 Structure and functional properties of filter paper separator

Filter paper is a fibrous material primarily composed of cellulose, a macromolecular polysaccharide formed by the

β-1,4-glycosidic bonding of glucose units. From a molecular structure perspective, filter paper consists of numerous interconnected six-membered glucose ring units, forming a complex pore network. This porous structure allows it to serve as a channel for ion transport while preventing direct contact between the electrodes, thus providing physical isolation (Fig. 1a).[84,85]

In AZBs, filter paper separators have been widely used in early research due to their low cost and ease of processing. However, they exhibit several critical drawbacks in practical applications:

Poor chemical stability: the primary component of filter paper, cellulose, is prone to degradation in strongly alkaline electrolytes (such as KOH), which compromises the separator's structure and impacts the long-term cycling stability of the battery.

Uneven pore size distribution: the pores of filter paper are relatively large and unevenly distributed, limiting its ability to physically block Zn dendrites, thus failing to effectively suppress dendrite growth. Once Zn dendrites penetrate the separator, they can cause internal short circuits, leading to battery failure.

Insufficient mechanical strength: after immersion in electrolyte, filter paper loses mechanical strength, becoming prone to rupture or deformation, which hinders its use in long-term cycling.

In summary, despite the low cost of filter paper separators, its poor chemical stability in strongly alkaline environments makes it unsuitable for high-performance AZBs.

3.2 Structure and functional properties of glass fiber (GF) separator

GF is an inorganic material primarily composed of SiO_2 (silicon dioxide), Al_2O_3 (aluminum oxide), CaO/MgO (calcium oxide/magnesium oxide), and B_2O_3 (boron oxide) (Fig. 1b).[86,87] These components impart excellent chemical and mechanical properties to GF:

Strong electrochemical corrosion resistance: during charge and discharge cycles, GF remains electrochemically inert, neither participating in redox reactions nor reacting with the electrolyte, thereby maintaining its structural integrity over time.

High porosity and excellent ion transport capability: GF separators typically have a porosity of 80–85%, providing an effective channel for Zn^{2+}, which reduces ion diffusion resistance and enhances the battery's rate capability.

Although GF separators exhibit several advantages, they also have certain limitations:

Ineffective Zn dendrite suppression: the pore size of GF separators is typically in the micron range, while the initial nucleation size of Zn dendrites can be as small as nanometers (<100 nm). Therefore, physical confinement alone is insufficient to prevent dendrite growth, which can still lead to short circuit issues.

Surface chemical inertia: the chemical surface of GF is relatively inert, limiting its ability to regulate the uniform deposition of Zn through adsorption or interface electric field control, which may exacerbate dendrite growth unevenness.

An ideal separator material should possess high mechanical strength, excellent chemical stability, a uniform pore structure, and good electrolyte wettability. While GF outperforms filter paper in chemical stability and electrochemical resistance, improvements are still needed in dendrite suppression.

3.3 Development timeline of separators for AZBs

In the early stages of AZBs research, filter paper was commonly used as the separator (Fig. 2) due to its low cost, simple structure, and easy accessibility in laboratory settings.[88–92] However, as research progressed and attention increasingly

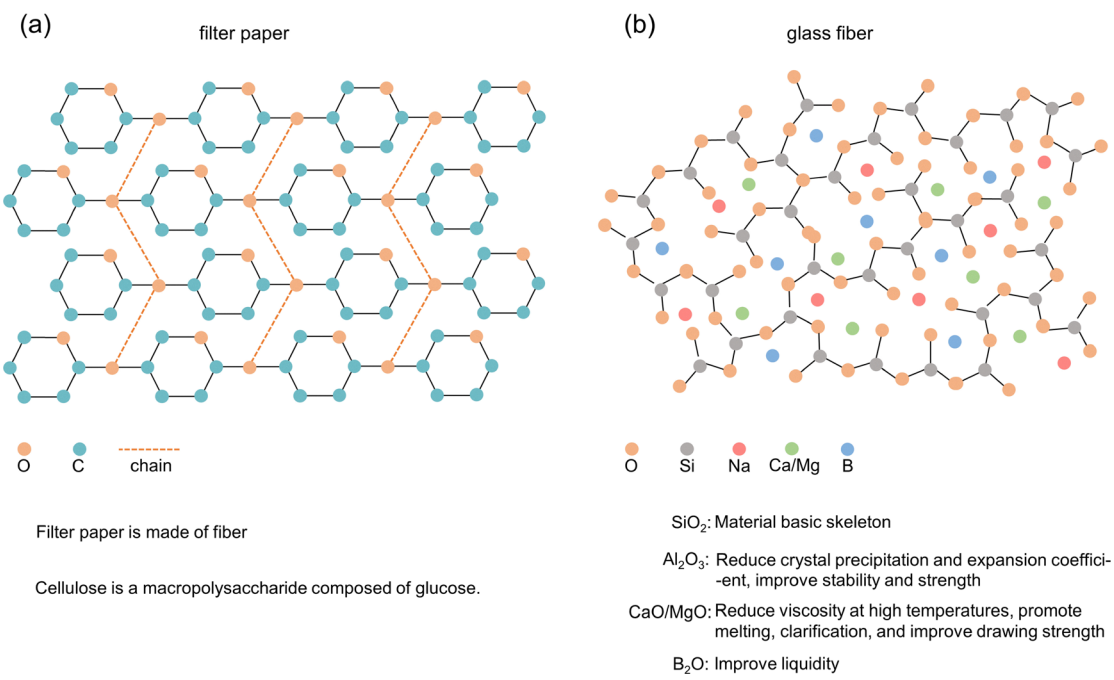

Fig. 1 Structural differences between filter paper (a) and GF (b).

focused on the Zn anode, the limitations of filter paper became apparent—particularly its low mechanical strength and limited thickness, which make it ineffective at blocking Zn dendrites. This can lead to short circuits and reduced battery safety. In contrast, GF separators offer several distinct advantages. The increased thickness confers improved resistance to dendrite penetration. Additionally, GF materials typically exhibit high porosity and excellent electrolyte wettability, which enhance ionic conductivity and electrolyte retention, thereby improving cycling stability and rate performance. As a result, GF has gradually replaced filter paper as a more widely used base material for separators in AZBs.

Nevertheless, GF alone still cannot fully address the challenges posed by both the anode and cathode, such as continuous dendrite growth, side reactions at the electrode interfaces, and poor ion selectivity of the separator. To overcome these issues, researchers have developed a variety of modification strategies based on GF, including surface coatings, functional treatments, and the incorporation of heterogeneous structures. At the same time, significant efforts have been made to design and develop novel high-performance separators aimed at fundamentally resolving the limitations of existing materials. Given the limitations of unmodified GF, extensive research efforts have been devoted to enhancing its performance and developing novel separators. In the following sections, I provide a comprehensive overview of recent progress in both GF modifications and the design of advanced separator materials.

4. GF separator modification strategies

The continuous growth of Zn dendrites is a major safety concern in AZBs. These needle-like structures can eventually pierce the separator, causing a short circuit that seriously affects the safety and lifespan of the battery. As shown in Fig. 3a, Zn dendrites grow inside the separator and can break through its structure, leading to short circuit failure. GF is a commonly used separator in AZBs because of its ability to hold electrolyte. However, it still has several problems during real use. For example, GF has a strong attraction to Zn^{2+}, which can guide dendrite growth toward the separator and increase the chance of short circuits.[93] In addition, as shown in Fig. 3b, GF cannot effectively stop the spreading and loss of cathode materials. This causes active material loss, faster self-discharge, and reduced battery capacity, which all speed up battery failure.

To address these issues, GF separators are typically modified to optimize their physical and chemical properties. This enables them to better suppress Zn dendrite growth, improve ion selectivity, and reduce side reactions, thus ensuring stable battery operation.

In AZBs, GF separator modification strategies are diverse. Different modification layer positions can meet various electrochemical needs, thereby optimizing battery performance. As an essential component of the battery, the separator is in direct contact with both the anode and cathode, and it can simultaneously regulate the chemical reactions at both electrode interfaces. Therefore, theoretically, separator modification holds the potential to address issues on both the cathode and Zn anode sides in a synergistic manner. Fig. 3c illustrates three common approaches to separator modification: modifying the layer near the anode side, the cathode side, or the full-separator.

The rationale behind our spatial classification is to highlight the functional asymmetry that naturally arises in AZB systems, where the anode and cathode experience significantly different electrochemical environments. Modifications on the anode side typically aim to suppress Zn dendrites and parasitic reactions (*e.g.*, hydrogen evolution), while those on the cathode side often target cathode dissolution, shuttle effects, or sluggish kinetics. Modifications applied to the entire separator are generally intended to address challenges on both sides simultaneously. Compared to previous reviews that mostly focus on material types or general functional effects, our spatially resolved framework offers a structure–function perspective that helps clarify where specific challenges arise and how targeted separator modifications can address them. By implementing these modification strategies, the performance of GF separators

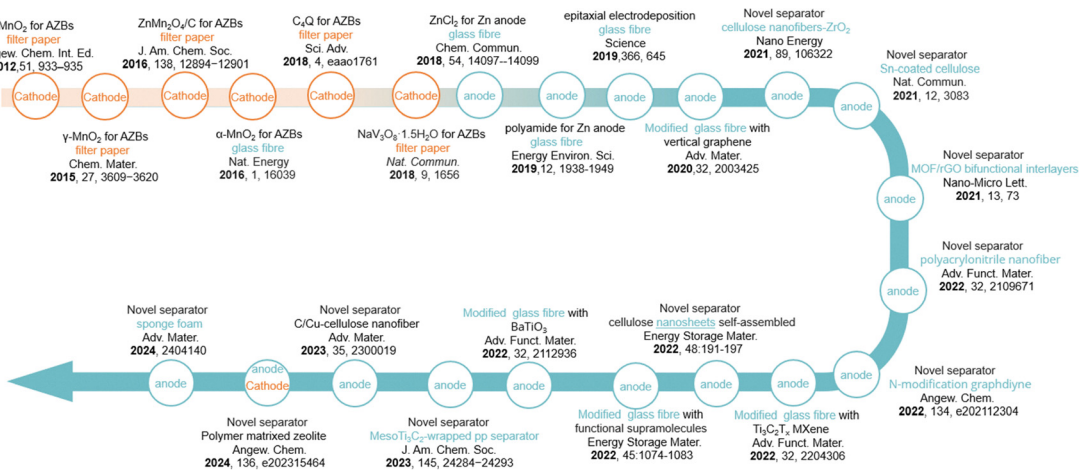

Fig. 2 The timeline outlines the development of separator materials for AZBs.

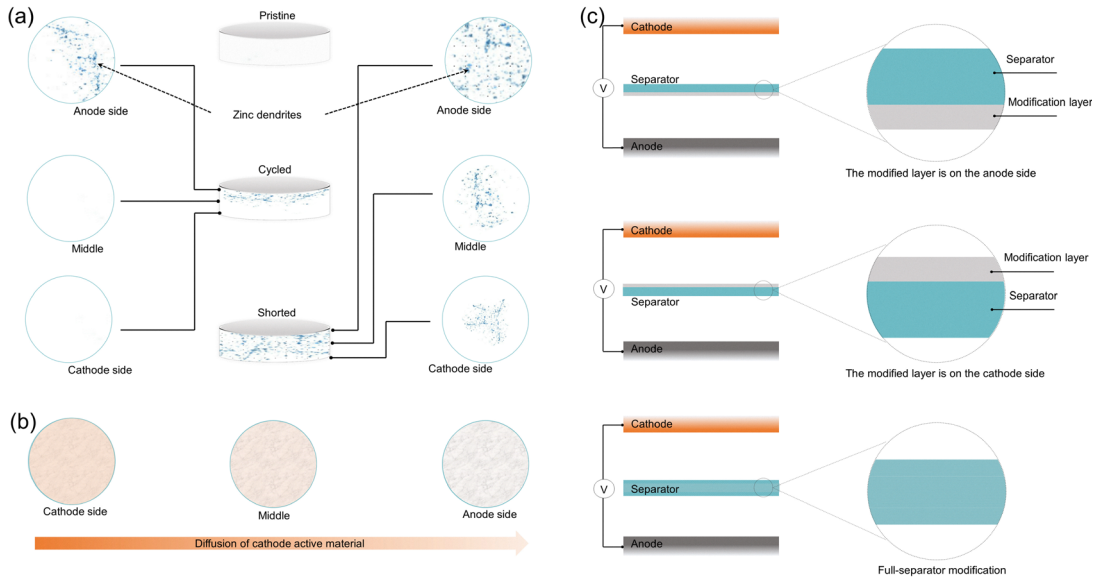

Fig. 3 (a) Distribution of Zn dendrites in the separator during battery cycling and short circuit. (b) Distribution of products dissolved by the cathode in the separator. (c) Current three methods of GF separator modification (anode side, cathode side, full-separator modification).

can be further enhanced, making them better suited for the requirements of AZBs.

4.1 Modification layer located on the anode side

In this design, the modification layer of the separator is oriented towards the Zn anode. This strategy is primarily employed to suppress Zn dendrite growth and prevent their penetration through the separator, which could otherwise cause battery internal short circuits. Typically, the materials used for the modification layer possess good Zn^{2+} affinity. These materials can induce uniform deposition of Zn, reducing the tip effect of dendrites. Additionally, the modification layer on the anode side can optimize the diffusion dynamics of Zn^{2+} through electric field regulation, improving the Coulombic efficiency and cycling stability of the battery.

This section reviews various strategies for separator modification on the anode side, including homogenizing the pore size distribution to regulate Zn^{2+} flux, employing Janus separators to optimize the interfacial electric field, and incorporating inorganic nanomaterials to enhance separator wettability while improving Zn^{2+} transport kinetics and deposition behavior. Through different material designs and engineering optimizations, these strategies have made significant progress in improving the stability of Zn anodes, suppressing dendrite growth, optimizing electrolyte wetting, and enhancing ion migration efficiency.

Furthermore, Liu *et al.*[94] designed a Halloysite nanotube (HNT)-modified glass fiber separator (HNT-GF, Fig. 4a), which further improves the performance of AZBs. As a natural inorganic mineral, HNT not only enhances the mechanical strength and puncture resistance of the separator but also homogenizes the pore size distribution (Fig. 4b), thereby optimizing the Zn^{2+} flux (Fig. 4c). More importantly, the unique electro-negativity differences between the inner and outer surfaces of HNT give the modified separator ion screening capability: the negatively charged outer surface stabilizes the Zn^{2+} flow, promoting multi-site progressive nucleation for uniform deposition, while the positively charged inner surface effectively traps and restricts the migration of SO_4^{2-}, serving as an "anion brake". As a result, the Zn^{2+} transference number of the HNT-GF separator increases to 0.71, effectively suppressing the passivation reaction on the anode surface and achieving dendrite-free, highly reversible Zn deposition. This strategy inspires the possibility of achieving specific ion screening and directional migration through surface chemical modifications or hetero structural designs, such as optimizing ion channels using positive/negative charge distribution, functional group regulation, or layered material structures.

The separator not only acts as a physical isolation layer but can also regulate the electric field distribution by introducing conductive networks or polar functional materials, optimizing the morphology of Zn^{2+} deposition and improving anode stability. Li *et al.*[95] developed a Janus separator by directly growing vertical graphene (VG) carpets on the anode side of commercial GF separators (Fig. 4e). Further, by using air plasma treatment to introduce oxygen and nitrogen heteroatoms onto the graphene surface, they formed a high surface area and porous three-dimensional VG framework. This design optimizes the electric field distribution at the anode/electrolyte interface, reducing the local current density and making the Zn^{2+} flux more uniform (Fig. 4f–k). This strategy not only has excellent scalability and cost-effectiveness but also serves as a general approach to optimize the stability of metal anodes in rechargeable batteries.

Although separator modification has proven to be an effective dendrite suppression strategy, current research pathways still face challenges in large-scale production, and there is a lack of focus on the fundamental mechanisms behind separator regulation. To address this, Su *et al.*[96] proposed a scalable MXene-modified Janus separator, which deposits $Ti_3C_2T_x$ MXene nanosheets on one side of commercial glass fiber (MXene-GF)

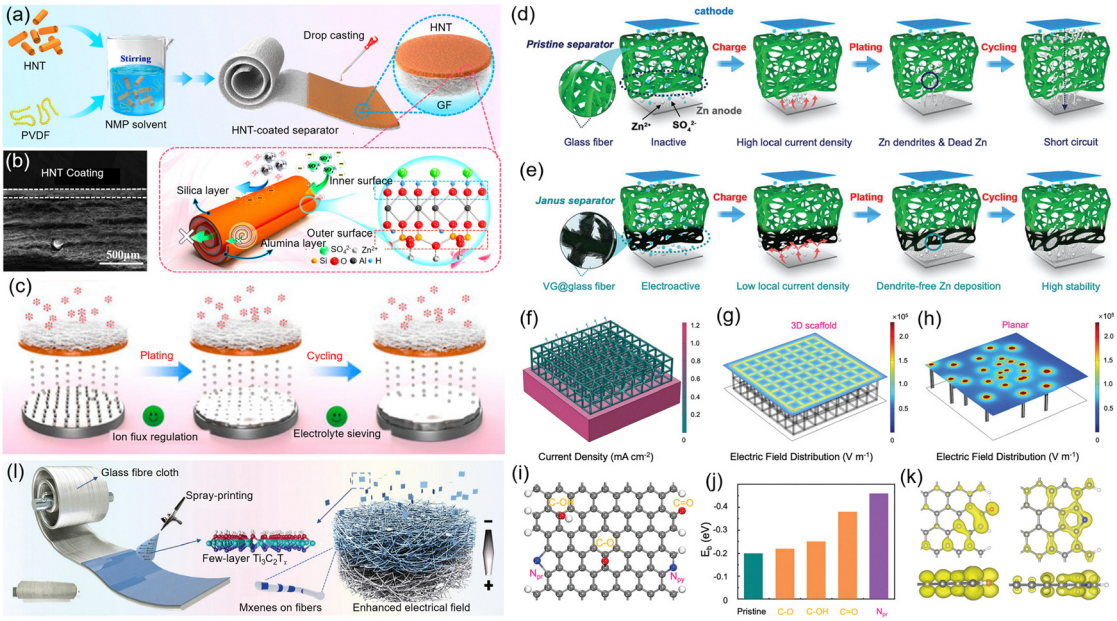

Fig. 4 (a) Schematic representation illustrating the fabrication process of the HNT-GF separator and the ion-sieving mechanism of HNT. (b) Cross-sectional SEM image showcasing the HNT-GF separator. (c) Diagrammatic depiction of Zn deposition behavior when using the HNT-GF separator. Schematic visualizations of the Janus separator concept designed for stabilizing the Zn anode. Reproduced with permission.[94] Copyright 2024, American Chemical Society. (d) Image of an unmodified GF separator and (e) a Janus separator featuring a vertically grown VG layer on one side, which aids in reducing local current density and ensuring uniform ion distribution. (f) Illustration of current distribution in the 3D scaffold. Electric field distribution of (g) the 3D scaffold structure (Janus separator) and (h) the 2D planar structure (pristine separator). DFT simulations of Zn adsorption on O/N-functionalized graphene: (i) structural configuration of O- and N-doped graphene, where gray, red, blue, and white represent carbon, oxygen, nitrogen, and hydrogen atoms, respectively. (j) Zn binding energy on O/N-functionalized graphene. (k) Yellow contours displaying the partial charge density around the Fermi level with an isosurface value of 0.002e bohr^{-3}, shown in top-view (upper) and side-view (lower) for C═O–G and C-Npr-G configurations (left to right). (l) Schematic representation of the fabrication process and functional mechanism of the MXene-GF separator. Reproduced with permission.[96] Copyright 2022 Wiley-VCH GmbH.

using a spray printing process (Fig. 4l). This method is not only simple and suitable for mass production but also imparts good electrolyte wettability, high ionic conductivity, and rich surface polar groups to the separator, thus optimizing Zn^{2+} transport dynamics and deposition behavior.

It is noteworthy that the MXene-GF separator has an adjustable dielectric constant (ε), with an optimized value of 53.5. This dielectric constant gradient can induce polarization in the GF through the Maxwell–Wagner effect, establishing a directional built-in electric field at the interface with 50% enhanced strength, accelerating Zn^{2+} migration and deposition dynamics. Therefore, this strategy can effectively stabilize the Zn anode, providing a uniform interface ion field, and offering a new direction and technical support for the development of high-performance AZBs.

4.2 Modification layer located on the cathode side

When the modification layer is positioned on the cathode side, its primary role is to optimize cathode reaction kinetics, suppress the dissolution and shuttling of active materials, and enhance the battery's cycling stability. This strategy is particularly critical in aqueous Zn–iodine (Zn–I_2) batteries. Zn–I_2 batteries have garnered widespread attention due to their high theoretical capacity ($\sim$211 mAh g^{-1}), cost-effectiveness, and the low toxicity of iodine.[97–99] However, in practical applications, this system faces challenges such as Zn dendrite growth, polyiodide (I_3^-/I_5^-) diffusion (Fig. 5a), and slow iodine redox kinetics. A common strategy to address polyiodide shuttling is interfacial engineering (Fig. 5a).[100] However, recent studies have shown that modifying the separator can also be highly effective. Bi *et al.*[101] proposed an innovative cathode-side interface engineering strategy by introducing cobalt-modified hollow nitrogen-doped MXene spheres (Co-HNMXS) on the cathode side of the GF separator (Fig. 5b). This material exhibits excellent interface hydrophilicity, ensuring fast ion transport. Additionally, the highly active Co–N–C sites effectively suppress polyiodide shuttling while accelerating the electrochemical conversion of iodine. This design not only enhances the redox kinetics of iodine but also reduces side reactions, effectively extending the battery lifespan. Yang *et al.*[102] reported a capture–adsorption–catalysis synergistic strategy, using Zn–Mn atomic pairs modified GF separators (ZnMn-NC/GF) to suppress self-discharge phenomena. The single Mn atomic sites were primarily responsible for adsorbing polyiodides, while the Zn–Mn atomic pairs promoted the conversion of iodine redox reaction intermediates (Fig. 5c and d). This strategy significantly improves the utilization of cathode active materials and demonstrating exceptional stability and long cycle life. Kang *et al.*[103] developed a Janus membrane with functional layers on both the anode and cathode sides to address multiple challenges

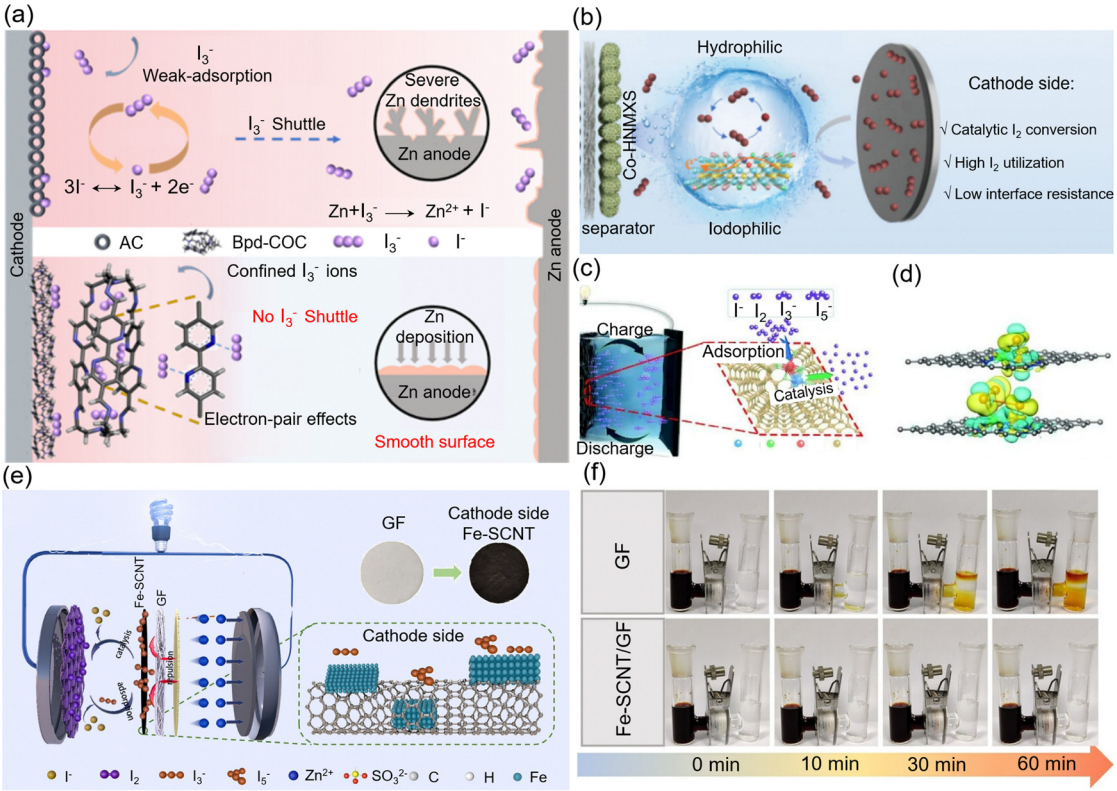

Fig. 5 (a) Schematic representation of the Zn metal anode corrosion mechanism induced by the I_3^- shuttle in AC-based AZBs, along with the inhibition mechanism of the I_3^- shuttle in Bpd-COC-based AZBs. Reproduced with permission.[100] Copyright 2024, Wiley-VCH. (b) Diagram illustrating the functional mechanism of the Co-HNMXS@GFA separator. Reproduced with permission.[101] Copyright 2025, Wiley-VCH. (c) Schematic visualization of the operational principles of a Zn-halogen battery incorporating a ZnMn-NC/GF separator. (d) Differential charge density mapping between I^-/I_3^- and ZnMn-N_6 sites. Reproduced with permission.[102] Copyright 2025, Wiley-VCH. (e) Schematic and basic characterization of the Fe-SCNT/GF separator. (f) Optical images showing the shuttle effect using H-type cells with I_3^-. Reproduced with permission.[103] Copyright 2023, Wiley-VCH.

associated with iodine cathodes. On the cathode side of a commercial glass fiber (GF) separator, they introduced a coating of Fe-decorated single-walled carbon nanotubes (Fe-SCNTs). This functional layer not only physically adsorbs polyiodide species and facilitates electron transport *via* the high surface area SCNTs, but also chemically adsorbs and catalyzes polyiodide through embedded Fe nanoparticles, thereby enhancing the redox reaction kinetics of iodine species (Fig. 5e). Through these synergistic effects, the Fe-SCNT cathode layer effectively anchors polyiodides and suppresses the shuttle effect (Fig. 5f), significantly improving the overall battery performance.

The successful implementation of cathode-side modification strategies provides new insights for enhancing the performance of AZBs. However, single modification strategies often address specific issues, and future research should focus on achieving multifunctional integration (such as simultaneously suppressing dendrite growth and polyiodide shuttling). Through continued optimization of cathode-side modification strategies, further improvements in the performance of AZBs can be achieved, promoting their development for practical applications.

In addition to directly optimizing cathode reaction kinetics, the cathode-side modification layer can also indirectly influence the behavior of the Zn anode through unique interfacial chemical interactions. Wu *et al.*[93] proposed a novel strategy to regulate Zn deposition by *in situ* modifying the cathode side of a commercial GF separator with polyaniline (PANI), forming a GF/PANI separator. In cells using the unmodified GF separator, the electric field at the Zn anode surface is unevenly distributed, which promotes the formation of Zn protrusions in the early stages of deposition. Moreover, the strong binding affinity between GF and Zn drives Zn^{2+} toward the separator, increasing the risk of dendrite penetration. In contrast, the PANI layer, rich in functional groups and with moderate Zn affinity, guides Zn^{2+} to deposit uniformly along the edge of Zn nuclei, resulting in a smooth Zn layer (Fig. 6a). The GF/PANI-600 separator provides balanced Zn affinity and a uniform electric field distribution, effectively directing homogeneous Zn deposition and suppressing dendrite growth through the PANI modification layer. Bu *et al.*[104] have moved beyond the traditional approach of passively inhibiting Zn dendrite growth and instead proposed an active dendrite digestion strategy. They modified separator with mesoporous Ti_3C_2 MXene (Meso Ti_3C_2), enabling it to actively participate in the oxidation and dissolution of dendrites during the battery's cycling process (Fig. 6b). This innovative design not only overcomes the limitations of traditional passive protective separators but also provides a new solution for stabilizing the Zn anode.

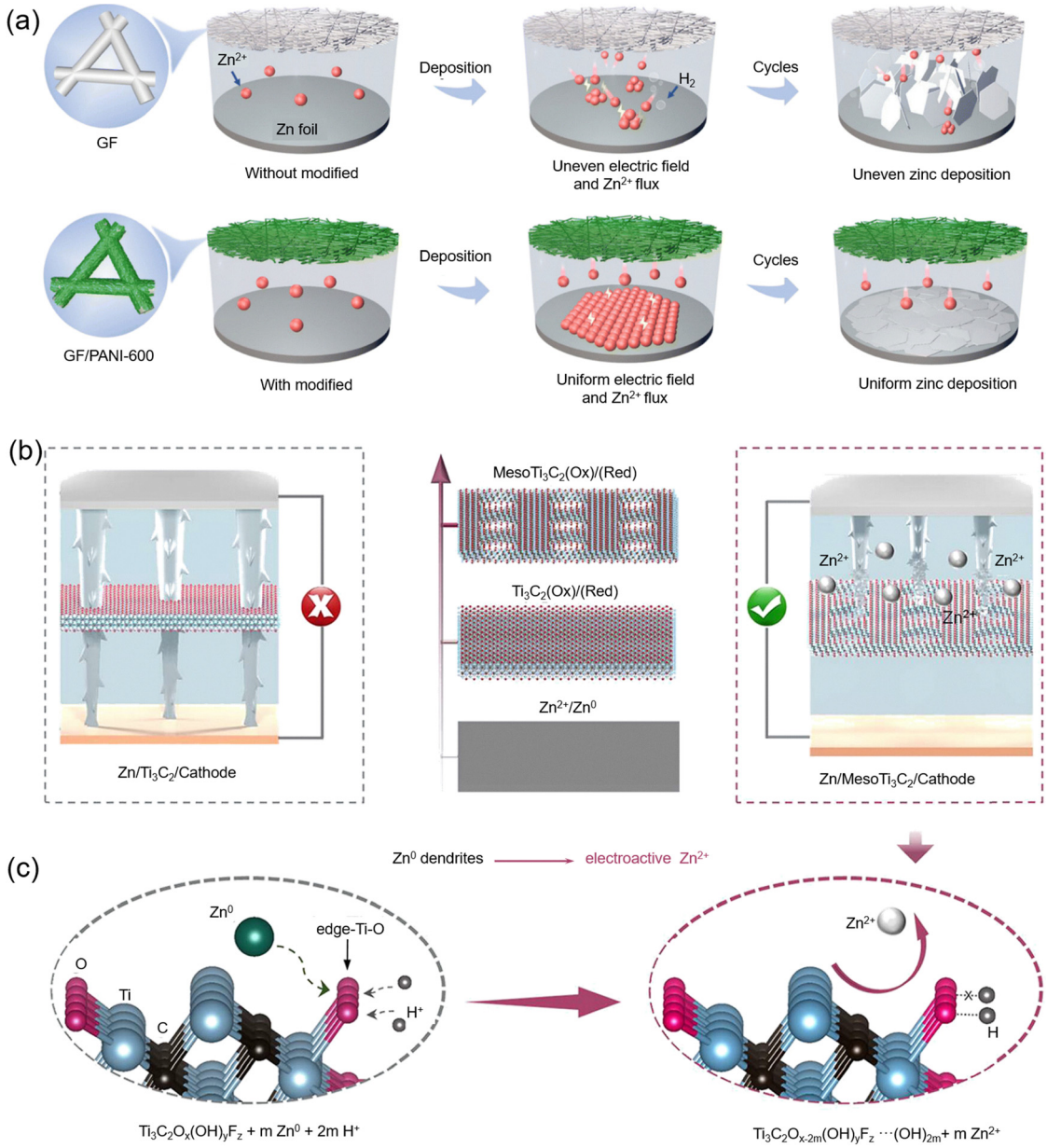

Fig. 6 (a) The schematic demonstration of the evolution of the plating process on Zn anodes with GF/PANI-600 and pristine GF separators. Reproduced with permission.[93] Copyright 2023, Royal Society of Chemistry. (b) Diagram illustrating the role of the meso Ti_3C_2-coated PP separator in suppressing Zn dendrite formation and the associated working mechanisms. (c) Spontaneous redox reaction occurring between Zn^0 and the Ti–O_e functional groups on meso Ti_3C_2. Reproduced with permission.[104] Copyright 2023, American Chemical Society.

Studies have shown that meso Ti_3C_2 has high oxidative properties, capable of spontaneously converting the dead Zn dendrites that have already formed back into Zn^{2+} ions through a redox process, which are then returned to the electrolyte to participate in electrochemical reactions (Fig. 6c). Compared to planar Zn dendrites, the edge-rich Ti–O sites of meso Ti_3C_2 can more effectively promote the oxidation of Zn dendrites and accelerate the electron transfer process. Therefore, under a practical working current density of 5 mA cm^{-2} and low overpotential (<50 mV), asymmetric cells can still cycle stably for 2200 hours, significantly extending the battery's lifespan. This study is the first to reveal the unique edge effect of mesoporous MXene materials and proposes an innovative active dendrite digestion method that ensures long-term operation of AZBs even when dendrites inevitably form.

The cathode-side modification layer strategy not only significantly enhances the performance of Zn–I_2 batteries but also provides new design directions for other aqueous metal batteries (such as Zn–VO*x*, Zn–air, *etc.*).[79,80,83] For example, in Zn–VO*x* batteries, similar modification layer designs can effectively suppress the dissolution of V; in Zn–air batteries, the modification layer can simultaneously optimize the kinetics of the oxygen reduction reaction (ORR) and oxygen evolution reaction (OER). These applications demonstrate the broad

applicability and scalability of the cathode-side modification layer strategy.

4.3 Full-separator modification

In this strategy, the full-separator substrate undergoes functional modification, with the modifier distributed throughout the separator. This approach focuses more on optimizing the overall battery performance rather than the modification of a single electrode. Full-separator modification can effectively regulate ion transport pathways, enhance electrolyte wettability, reduce internal resistance, and inhibit dendrite growth. Additionally, this method can balance local current density, thereby improving the battery's rate performance and long-term cycling stability. Full-separator modification mainly includes two forms: uniform modification of the full-separator and gradient modification of the full-separator. Due to the slow ion transport rate on the surface of the Zn anode, large concentration gradients are easily formed, leading to uneven Zn^{2+} flux distribution, especially under high current density conditions, which can easily trigger dendrite growth. To address this, Tan *et al.*[105] proposed a simple and efficient separator engineering strategy—introducing an ion acceleration layer to regulate Zn^{2+} flux and achieve dendrite-free deposition (Fig. 7a and b). In this strategy, ZnHCF (Zn hexacyanoferrate complex) is used as a modifier. With its excellent Zn affinity and efficient ion diffusion channels, it can quickly capture Zn^{2+} and guide its uniform deposition. The ion acceleration layer can improve the conductivity of Zn^{2+}, reduce the activation energy of the deposition process, and effectively regulate the Zn^{2+} concentration gradient, thereby inducing uniform distribution of Zn^{2+} (Fig. 7c and d). Under this optimized strategy, Zn‖Zn symmetric cells can stably cycle for 2700 hours at a current density of 2 mA cm^{-2}, and 1770 hours at a high current density of 10 mA cm^{-2}. Furthermore, the modified separator significantly improves the overall battery's cycle life and rate performance, fully verifying its advantages in practical applications. Future separator designs can draw from this concept to explore new materials with higher Zn affinity and fast ion transport capabilities (such as MOFs, Prussian blue materials, 2D nanomaterials, *etc.*) to further optimize ion migration.

Song *et al.*[106] proposed a Zr-based MOF functionalized separator (UiO-66-GF) (Fig. 7e). In this design, the UiO-66 MOF, through its confinement effect, uniformly distributes Zn^{2+} flux, enhances Zn^{2+} transport at the separator–anode interface, and effectively regulates the electric field distribution on the Zn anode surface (Fig. 7f). Additionally, UiO-66-GF induces Zn^{2+} deposition to preferentially grow along the (002) crystallographic plane, thereby inhibiting dendrite formation and side reactions. The (002) plane has a weak adsorption effect

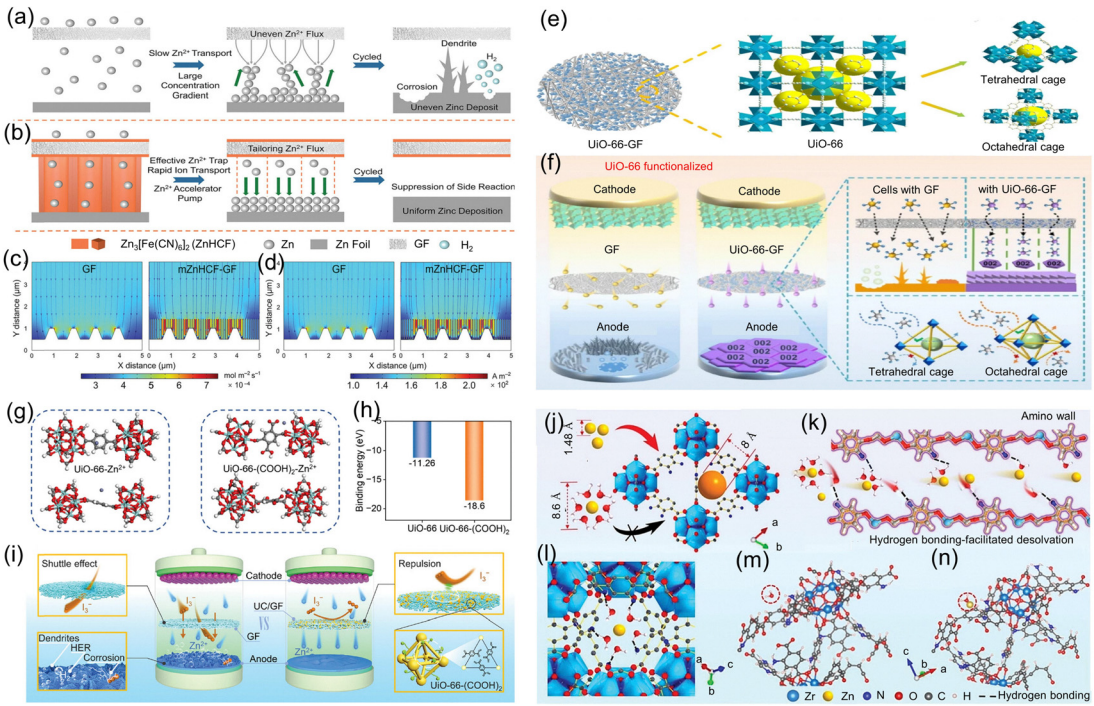

Fig. 7 Design of the ZnHCF–GF separator. Schematic depiction of the Zn^{2+} deposition process using different separators: (a) GF and (b) ZnHCF–GF. COMSOL simulations illustrating (c) Zn^{2+} flux and (d) current density distribution on the Zn electrode with GF and ZnHCF–GF separators. Reproduced with permission.[105] Copyright 2024, Wiley-VCH. (e) Structural representation of UiO-66 and its fundamental role in regulating Zn^{2+} ion coordination and migration. (f) Schematic diagram of AZBs assembled with commercial GF and UiO-66-GF separators. Reproduced with permission.[106] Copyright 2022, Elsevier. Computational models evaluating the interaction between Zn^{2+} ions and (g) UiO-66/UiO-66-$(COOH)_2$. (h) Binding energy comparison of Zn^{2+} ions with UiO-66 and UiO-66-$(COOH)_2$. (i) Schematic representation of AZBs incorporating commercial GF and UC/GF separators. Reproduced with permission.[107] Copyright 2024, Wiley-VCH. (j) Comparison between the Zn^{2+} ion size and the pore size of UiO-66-NH_2. (k) and (l) Graphical depiction of hydrogen bonding interactions between H_2O molecules and $-NH_2$ groups in UiO-66-NH_2 from different perspectives. (m) H_2O adsorption model and (n) H_2O–Zn^{2+} adsorption model for UiO-66-NH_2. Reproduced with permission.[108] Copyright 2023, Wiley-VCH.

on H^+, further reducing hydrogen evolution and corrosion side reactions, thus improving the battery's corrosion resistance. Ultimately, this strategy constructs an ultra-stable Zn anode and high-performance AZB, with symmetric cells exhibiting highly reversible electroplating/stripping behavior, a cycle life exceeding 1650 hours, and the full-cell cycling 1000 times at a current density of 1.0 A g^{-1} with a capacity retention rate of 85%, demonstrating excellent long-term cycling stability.

MOFs, as a type of porous and stable functional material, have significant potential in constructing ion-selective separators, particularly due to their tunable crystal structures, which make it easy to introduce various functional groups (such as –COOH, $–NH_2$, *etc.*), enhancing their interaction with electrolyte components and improving separator ion conductivity and selectivity. For example, Yang *et al.*[107] used carboxyl-functionalized Zr-based MOFs (UiO-66-$(COOH)_2$, abbreviated as UC) to modify a separator and constructed a multifunctional UC/GF separator (Fig. 7g–i). This separator achieves dual regulation of both the anode and cathode in AZBs: on the one hand, the Zn- and water-affinity properties of the carboxyl group can effectively adsorb Zn^{2+}, promote Zn^{2+} migration, and accelerate the desolvation process of hydrated Zn^{2+}, improving the uniformity of Zn^{2+} flow and reducing corrosion and HER; on the other hand, the electrostatic repulsion between carboxyl groups and polyiodides can effectively inhibit the shuttle effect, reducing the loss of cathode active material and severe Zn corrosion (Fig. 7g–i).

Ma *et al.*[108] further investigated the modification effect of amino ($–NH_2$)-functionalized Zr-based MOFs (UiO-66-NH_2) on the separator and incorporated it into a cellulose-based separator. The study found that the amino group not only exhibits good Zn affinity but also forms strong interactions with H_2O molecules through hydrogen bonds, allowing the subnano-sized channels inside UiO-66-NH_2 to act as a desolvation sieve, increasing the Zn^{2+} migration rate and optimizing its distribution (Fig. 7j–n). Even with an ultra-thin separator of only 20 μm, the modified separator still significantly enhances the reversibility of Zn electrochemistry and effectively suppresses HER induced by water.

The uniform full-separator modification strategy can effectively enhance the cycle life and rate performance of AZBs by regulating Zn^{2+} transport, optimizing deposition morphology, and reducing side reactions. In the future, functionalized separators based on MOFs, Prussian blue materials, and other efficient ion-transport materials still have vast research potential and could provide new ideas and solutions for the development of AZBs.

Tian *et al.*[109] proposed an ion gradient separator for stabilizing the dual-electrode structure of AZBs (Fig. 8a). Compared to traditional GF separators, this gradient separator forms a low Zn^{2+} concentration region near the cathode and a high Zn^{2+} concentration region near the anode, thus optimizing overall battery performance. In the low Zn^{2+} concentration region, the $NH_4V_4O_{10}$ (NVO) model cathode maintains good electrolyte wettability, ensuring smooth ion transport. Meanwhile, *N*-methyl pyrrolidone (NMP), diffusing from the high Zn^{2+} concentration region to the cathode, can regulate the solvent structure of the electrolyte, promoting the formation of a stable cathode–electrolyte interface (CEI) rich in N/ZnS/ZnF_2, which effectively inhibits the dissolution of vanadium(v) (Fig. 8b and c). Additionally, the presence of the high Zn^{2+} concentration region synergistically interacts with the solid electrolyte interface (SEI) formed at the anode, significantly suppressing Zn dendrite growth and side reactions. Importantly, this high Zn^{2+} concentration region also effectively prevents vanadium ion diffusion toward the anode, thus improving the reversibility of Zn plating/stripping (Fig. 8d and e).

On the other hand, Liang *et al.*[110] introduced $BaTiO_3$ (BTO) nanoparticles into a GF separator, utilizing their excellent Zn affinity and spontaneous polarization effect to regulate Zn^{2+} transport behavior (Fig. 8f). The BTO nanoparticles exhibit a gradient distribution within the GF separator—anchoring to the fiber surface within the separator to enhance Zn^{2+} transport efficiency at the electrolyte-fiber interface; and near the Zn anode, the BTO nanoparticles not only anchor to the fibers but also fill the fiber gaps, regulating the uniform distribution of Zn^{2+} at the separator–Zn anode interface, reducing local current density nonuniformity. Moreover, studies show that the BTO (110) crystallographic plane has the strongest adsorption ability for Zn atoms (Fig. 8g and j), superior to many known Zn-affinity materials, further verifying the excellent performance of BTO particles in capturing Zn^{2+}.

Different separator modification strategies are suitable for different types of AZBs. By rationally designing the types and distribution positions of modification layers, it is possible to effectively optimize the electrolyte environment, balance ions flux, and stabilize electrode interfaces, thereby significantly enhancing the battery's cycle life and rate performance. These research findings provide important theoretical support and technical guidance for the development of high-performance AZBs and are expected to drive the commercialization of next-generation energy storage devices.

The reported effects of modified GF separators are summarized in Table 1. These separators have demonstrated excellent capacity retention and enhanced cycling stability across a range of AZBs. The incorporation of functional layers onto GF separators effectively regulates Zn^{2+} flux, suppresses dendrite growth, and promotes uniform Zn deposition. In many cases, the modified GF structure also contributes to mitigating parasitic reactions, such as hydrogen evolution, thereby improving Coulombic efficiency and extending battery lifespan. While current studies primarily explore a limited set of modification strategies and functional materials, the promising performance outcomes highlight the substantial potential of this approach. These strategies typically involve physical coating, chemical grafting, or *in situ* formation of inorganic or polymeric layers, each contributing specific benefits such as enhanced ionic conductivity, mechanical robustness, or interfacial stability.

To support the practical deployment of these strategies, a deeper understanding of their long-term performance and electrode compatibility is essential. In this context, we provide a critical evaluation of key considerations for functional layer coatings and asymmetric separator designs: (a) chemical and electrochemical stability under cycling. Functional layers

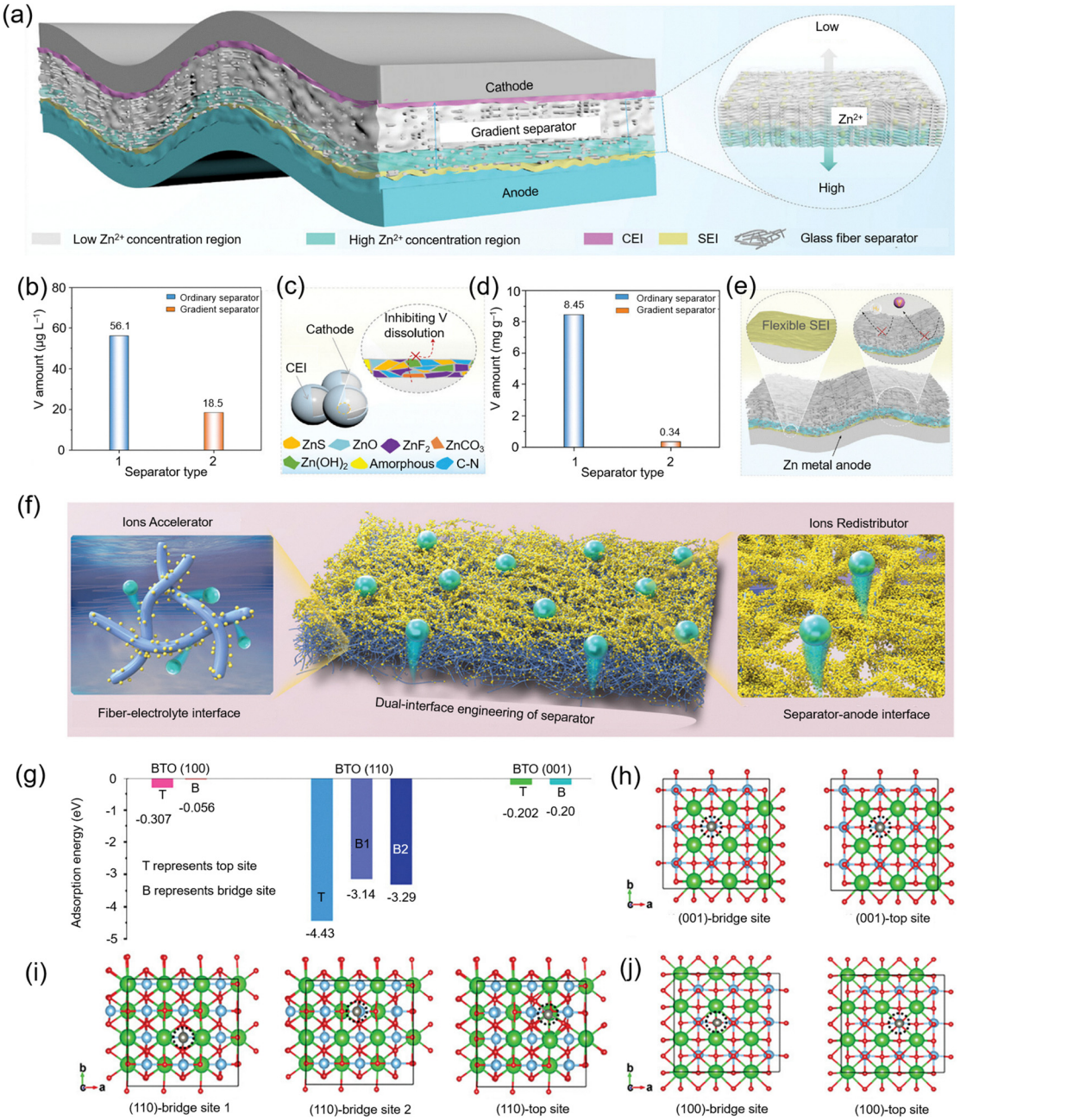

Fig. 8 (a) Schematic representation of a Zn metal battery incorporating a gradient separator. (b) Analysis of vanadium(v) content in the electrolyte after 100 cycles. (c) Diagram illustrating the role of the gradient separator on the cathode. (d) *V* concentration on the surface of the anode. (e) Mechanistic illustration of the interface chemistry between the gradient separator and the Zn metal anode. Reproduced with permission.[109] Copyright 2024, Wiley-VCH. (f) Schematic diagram showcasing dual-interface engineering in separators. (g) Binding energy between a Zn atom and various adsorption sites of BTO. (h) Top view of the geometric configuration for Zn atom adsorption on the BTO(001) plane, (i) BTO(110) plane, and (j) BTO(100) plane. Reproduced with permission.[110] Copyright 2022, Wiley-VCH.

(*e.g.*, metal oxides, polymers, or 2D materials) and asymmetric separators often show promising initial performance but may undergo structural degradation or chemical transformation over prolonged cycling. For instance:

Zincophilic or zincophobic coatings may lose functionality due to side reactions with Zn^{2+} or electrolyte decomposition products. Polymeric coatings (*e.g.*, PEO, PTFE) may swell, dissolve, or degrade in mildly acidic/neutral electrolytes, especially over hundreds of cycles. Metal oxide layers (*e.g.*, TiO_2, Al_2O_3) can experience cracking or delamination under repeated volume expansion/contraction at the Zn anode. We emphasize the need for accelerated aging tests, such as high-rate or high-temperature cycling, to simulate realistic degradation pathways and better assess durability. (b) Interfacial compatibility with both electrodes. While asymmetric separators are tailored to optimize interfacial behavior on both the anode and cathode sides, mismatched

Table 1 Summary of GF separator modification strategies, functions, and electrochemical performance

Separator Ref.	Working mechanisms	Electrolyte Zn‖Zn performance	Full cells performance
HNT@GF[94]	• Enhancement of mechanical strength • Homogenization of pore size distribution • Optimization of Zn^{2+} flux	2 M $ZnSO_4$ (+0.1 M $MnSO_4$) 3000 h (1 mA cm^{-2}; 1 mAh cm^{-2}) 2000 h (5 mA cm^{-2}; 1 mAh cm^{-2})	Zn‖MnO_2 1000 cycles 2 A g^{-1}; 93.4%
VG@GF[95]	• Optimization of electric field distribution • Reduction of local current density • Uniform Zn^{2+} flux distribution	2 M $ZnSO_4$ 300 h (0.5 mA cm^{-2}; 0.5 mAh cm^{-2}) 600 h (10 mA cm^{-2}; 1 mAh cm^{-2})	Zn‖AC 5000 cycles 5 A g^{-1}; 93%
$Ti_3C_2T_x$ MXene @GF[96]	• Built-in electric field • Good electrolyte wettability • Homogenization of local current	2 M $ZnSO_4$ 1180 h (1 mA cm^{-2}; 1 mAh cm^{-2}) 250 h (5 mA cm^{-2}; 5 mAh cm^{-2})	Zn‖KVOH 1000 cycles 5 A g^{-1}; 77.9%
Gra-CeF3@GF[111]	• Tailored Zn^{2+} flux • Suppressed SO_4^{2-} transport • Suppression of side reactions	2 M $ZnSO_4$ 2500 h (1 mA cm^{-2}; 1 mAh cm^{-2}) 1000 h (5 mA cm^{-2}; 5 mAh cm^{-2})	Zn‖V_2O_5 2000 cycles 2 A g^{-1}; —
Co-HNMXS@GF[101]	• Inhibition of polyiodide shuttling • Promotion of iodine conversion	Catholyte (0.1 M I_2 + 1 M LiI) anolyte (2 M $ZnSO_4$) 2900 h (1 mA cm^{-2}; 1 mAh cm^{-2})	Zn‖I_2 20 000 cycles 2 A g^{-1}; 80%
ZnMn-NC@GF[102]	• Efficient polyiodide adsorption • Accelerated intermediate conversion	2 M $ZnSO_4$	Zn‖I_2 30 000 cycles 5 A g^{-1}; 95%
SCNT@GF[112]	• Effective polyiodide anchoring • Catalysis of iodine redox kinetics	1 M $ZnSO_4$ 2500 h (1 mA cm^{-2}; 1 mAh cm^{-2})	Zn‖I_2 30 000 cycles 5 A g^{-1}; 76%
GO@GF[113]	• Inhibit dendrite growth	3 M Zn $(CF_3SO_3)_2$ 480 h (1 mA cm^{-2}; 0. 5 mAh cm^{-2})	Zn‖PAVO 4800 cycles 5 A g^{-1}; 74%
SR-P@GF[114]	• Enhanced Zn ion transport • Promotion of uniform Zn deposition • Assistance in desolvation of Zn^{2+}	2 M $ZnSO_4$ (+0.2 M $MnSO_4$) 500 h (1 mA cm^{-2}; 1 mAh cm^{-2})	Zn‖MnO_2 1000 cycles 1 A g^{-1}; 73.9%
PANI@GF[93]	• Weakens zincophilicity • Homogenization of surface electric field • Promotion of uniform Zn Ion stripping	2 M $ZnSO_4$ 3000 h (1 mA cm^{-2}; 1 mAh cm^{-2})	Zn‖MnO_2 300 cycles 0.5 A g^{-1}; 89.5%
ZnHCF@GF[105]	• Fast Zn^{2+} trapping • Quick Zn^{2+} delivery	2 M $ZnSO_4$ 2700 h (2 mA cm^{-2}; 1 mAh cm^{-2}) 1750 h (10 mA cm^{-2}; 2 mAh cm^{-2})	Zn‖AC 20 000, 1 A g^{-1}; 95.8%
UiO-66@GF[106]	• Enhanced charge carrier transport • Improved corrosion resistance • Promotion of dendrite-free	2 M $ZnSO_4$ (+0.1 M $MnSO_4$) 1650 h (2 mA cm^{-2}; 1 mAh cm^{-2})	Zn‖MnO_2 1000 cycles 1 A g^{-1}; 85%
UiO-66-$(COOH)_2$@GF[107]	• Facilitated Zn^{2+} transport • Accelerated desolvation of Zn^{2+} • Suppressed polyiodide transfer	2 M $ZnSO_4$ 3400 h (5 mA cm^{-2}; 1 mAh cm^{-2})	Zn‖I_2 3600 cycles 1 C; 72.3%
UiO-66-NH_2@GF[108]	• Zn^{2+} desolvation sieves • Facilitated Zn^{2+} migration • Uniform distribution of Zn^{2+}	2 M $ZnSO_4$ (+0.2 M $MnSO_4$) 2000 h (2 mA cm^{-2}; 2 mAh cm^{-2})	Zn‖MnO_2 1000 cycles 1 A g^{-1}; 95.1%
Gra@GF[109]	• Inhibition of dendrite growth • Prevention of V ion diffusion	1 M Zn $(OTf)_2$ 4800 h (3 mA cm^{-2}; 1 mAh cm^{-2})	Zn‖NVO 800 cycles 1 A g^{-1}; 88.1%
BTO@GF[110]	• Accelerated Zn^{2+} transport • Homogenization of ion transport	2 M $ZnSO_4$ (+0.2 M $MnSO_4$) 1600 h (10 mA cm^{-2}; 2.5 mAh cm^{-2})	Zn‖MnO_2 1800 cycles 1 A g^{-1}; —
GFNs-PVDF@GF[115]	• Homogenization of Zn^{2+} transport • Suppression of SO_4^{2-} flux • Inhibition of Zn dendrite	2 M $ZnSO_4$ 1800 h (1 mA cm^{-2}; 1 mAh cm^{-2})	Zn‖MnO_2 100 cycles 0.2 A g^{-1}; 90%
NDs@GF[116]	• Regulation of separator pore structure	2 M $ZnSO_4$ (+0.2 M $MnSO_4$)	Zn‖MnO_2

Table 1 (*continued*)

Separator Ref.	Working mechanisms	Electrolyte Zn‖Zn performance	Full cells performance
	• Control of Zn^{2+} transport properties	1800 h (5 mA cm^{-2}; 1 mAh cm^{-2})	1000 cycles 1 A g^{-1}; —
Cu(II)/PAD@GF[117]	• Improved water absorption capability • Optimized ion transport pathways	2 M $ZnSO_4$ 1800 h (1 mA cm^{-2}; 1 mAh cm^{-2})	Zn‖V_2O_5 1000 cycles 2 A g^{-1}; —
SA@GF[118]	• Lower Zn^{2+} desolvation barrier • No concentration polarization • Enhanced Zn^{2+} transport efficiency	2 M $ZnSO_4$ 1230 h (1 mA cm^{-2}; 1 mAh cm^{-2})	Zn‖MnO_2 500 cycles 1 A g^{-1}; 70.4%
SnF2@GF[119]	• Homogenization of Zn^{2+} flux • Suppression of byproduct formation 1400 h (1 mA cm^{-2}; 1 mAh cm^{-2}) 1000 h (5 mA cm^{-2}; 1 mAh cm^{-2})	2 M $ZnSO_4$	Zn‖MnO_2 200 cycles 1 A g^{-1}; 80%
ZLB@GF[120]	• Uniform electric field • Uniform Zn^{2+} deposition	2 M $ZnSO_4$ 3200 h (10 mA cm^{-2}; 10 mAh cm^{-2})	Zn‖MnO_2 2000 cycles 0.5 A g^{-1}; 76.7%

chemical environments pose risks. On the anode side, functional layers must accommodate Zn plating/stripping dynamics without impeding ion transport or triggering dendrite growth. On the cathode side, coatings must tolerate oxidative environments and avoid dissolution or passivation effects that would impede redox kinetics. Importantly, some materials (*e.g.*, redox-active interlayers, or organic functional groups) can unintentionally catalyze parasitic reactions or shuttle effects if not properly confined or stabilized. (c) Mechanical and dimensional stability. Separator coatings are also subjected to physical stresses such as swelling/deswelling and electrode volume changes, all of which can lead to mechanical failure or interfacial delamination. Strategies like polymer cross-linking, gradient interface design, and *in situ* polymerization are increasingly applied to enhance mechanical integrity, though their long-term reliability requires further validation. (d) Scalability and manufacturability.

Lastly, while many interfacial designs are effective at the laboratory scale, their practical application may be constrained by synthesis complexity, cost, or scalability. For example, solution casting of ultrathin layers can suffer from reproducibility issues and limited throughput. To facilitate real-world implementation, scalable manufacturing methods such as spray-coating, roll-to-roll lamination, and electrospinning should be prioritized. These considerations underscore the importance of integrating materials design with durability testing and scalable processing to bridge the gap between laboratory demonstrations and commercial viability.

It is important to note that while separator and electrode coating technologies often employ similar materials—such as metal–organic frameworks (MOFs), carbon nanotubes (CNTs), MXene, conductive polymers, and transition metal compounds—their functional roles and operating environments are fundamentally different. Both strategies are essential for advancing high-performance AZBs, but they involve distinct design principles and mechanisms of action.

Despite their differences, these coatings share a common goal: to stabilize the electrochemical environment and enhance overall battery performance. They contribute to suppressing Zn dendrite growth, promoting uniform Zn^{2+} distribution and deposition, and reducing parasitic side reactions such as hydrogen evolution and corrosion. These enhancements are particularly vital in aqueous systems, where challenges like water decomposition and metal dissolution can severely impact cycle life and Coulombic efficiency.

Separator coatings are applied to the surface of commercial or custom-designed separators—typically porous polymeric or glass fiber membranes—that serve as physical barriers between the anode and cathode. The coating layer is designed to perform several important functions beyond the general roles mentioned above. First and foremost, separator coatings regulate ion transport by modulating the local electric field and controlling Zn^{2+} flux. This helps to avoid the formation of high-concentration gradients that can lead to uneven plating and dendrite nucleation. Secondly, separator coatings play a critical role in inhibiting shuttle effects. For example, in Zn–iodine or Zn–organic batteries, soluble redox-active species such as polyiodides or small organic molecules can migrate between the electrodes, causing capacity loss and self-discharge. Coatings with adsorption capabilities—such as those based on MOFs, metal oxides, or nitrogen-doped carbon—can trap these shuttle species and reduce crossover, thereby improving cycling stability. Thirdly, separator coatings reinforce the mechanical integrity and chemical stability of the separator itself. In aggressive electrochemical environments, uncoated separators may degrade, lose dimensional stability, or become perforated by Zn dendrites. Functional coatings can serve as protective barriers, increasing the separator's resistance to chemical attack and enhancing its ability to block dendrite penetration.

On the other hand, electrode coatings are typically applied directly to the surface of the Zn anode (or, to the cathode) and are designed to interface directly with the electrolyte during charge–discharge cycles. These coatings often focus on improving electronic conductivity, particularly in cases where the Zn surface

becomes passivated by insulating by-products. Conductive materials such as CNTs, graphene, or MXene can help to establish an electronically conductive network across the anode surface, ensuring uniform current distribution and reducing localized current hotspots that accelerate dendrite growth. Moreover, electrode coatings help to guide the nucleation and growth of Zn during plating. By engineering a surface with appropriate zincophilicity—using materials like ZnO, Sn, or organic functional groups—it is possible to lower the nucleation barrier and achieve more uniform Zn deposition. This reduces the likelihood of uncontrolled dendrite formation and promotes a dense Zn layert.

Electrode coatings can also act as artificial solid–electrolyte interfaces (SEIs), especially in mildly acidic or neutral aqueous electrolytes where traditional SEI layers are either unstable or nonexistent. These engineered interfaces serve to regulate interfacial ion transport, suppress side reactions such as hydrogen evolution, and prolong the lifetime of the Zn anode. Compared to separator coatings, electrode coatings face harsher chemical and electrochemical conditions, including direct exposure to redox reactions and fluctuating pH levels at the electrode surface.

While the materials used in separator and electrode coatings often overlap, their performance metrics and evaluation methods are quite different. Separator coatings are usually assessed based on ionic conductivity, transference number, permeability to shuttle species, and dendrite-blocking ability. Electrode coatings, on the other hand, are evaluated based on their ability to reduce overpotential, lower the nucleation voltage, improve Coulombic efficiency, and extend cycle life.

In conclusion, both separator and electrode coatings are essential tools in overcoming the inherent challenges of AZBs. While they may employ similar materials, their functional purposes, physical locations in the cell, and operational demands differ markedly. Separator coatings primarily modulate ion transport and protect the separator from chemical/mechanical failure, while electrode coatings directly stabilize the anode interface and control the dynamics of Zn deposition. For next-generation AZBs, a synergistic design that integrates both coating strategies could offer a comprehensive solution to long-standing issues such as dendrite formation, low efficiency, and limited lifespan.

5. Novel separators

In addition to the previously mentioned materials, in recent years, several novel separator materials have been researched and applied. These separators not only focus on the optimization of a single electrode but also emphasize the synergistic regulation of both the anode and cathode performance, thereby significantly improving the full cells cycle stability. Here, a ''Novel Separator'' refers to separators that are synthesized from scratch using new or hybrid materials without relying on commercial substrates, often involving new membrane formation processes such as filtration, casting, or *in situ* polymerization.

5.1 Polymer-based separators

Polymer materials show great potential for use in separators for AZBs due to their excellent mechanical strength, flexibility, and chemical stability. They can effectively separate the anode and cathode, preventing Zn dendrites from piercing through and causing short circuits. In addition, by adjusting their structure and functional groups, polymer materials can help guide the movement of Zn^{2+}, suppress dendrite growth, and reduce side reactions, thereby improving the battery's cycling stability and safety. Polymers are also easy to process and can be combined with inorganic fillers or conductive polymers to create multifunctional composite separators. Moreover, polymer materials are made from widely available raw materials, have mature manufacturing processes, and are relatively low in cost, making them suitable for large-scale production and commercial applications. As a result, they have become a key focus in the development of high-performance separators for AZBs.

Yuan *et al.*[121] developed a simple dip-coating method to uniformly composite a polycationic polymer composed of poly(diallyl dimethyl ammonium) (PDDA) cations and bis(trifluoromethanesulfonyl)imide (TFSI) anions onto a GF separator (Fig. 9a and b). The PDDA cations strongly adsorb polyiodide anions, effectively inhibiting the shuttle effect of polyiodides (Fig. 9c). Moreover, the hydrophobicity of the PT@GF separator allows it to closely contact the Zn anode, forming a water-deficient electrical double-layer (EDL) interface, reducing corrosion of Zn and suppressing HER (Fig. 9d). Simultaneously, the polycation evenly regulates the electric field distribution at the anode surface, inhibiting the tip effect and effectively suppressing the growth of Zn dendrites (Fig. 9e). Thanks to this optimized design, batteries using the PT@GF separator exhibit excellent long-cycle stability.

Huang *et al.*[122] designed a modified PAN (polyacrylonitrile) nanofiber separator using electrospinning technology, with PAN and a zwitterionic surfactant (sulfobetaine methacrylate, SBMA) as the starting materials (Fig. 9f–h). The SBMA, which contains sulfonic acid groups ($-SO_3^-$), can change the physical properties of the precursor solution and influence the electric field during the electrospinning process. Moreover, it helps regulate the distribution of Zn^{2+} by reducing concentration polarization caused by polar groups on the Zn surface (Fig. 9i–l). This leads to a more uniform electric field and smoother ion movement. This work presents a simple and effective approach to designing a PAN-based functional separator with a high ion transference number, which can guide Zn^{2+} deposition and improve the performance of AZBs. Yang *et al.*[123] demonstrated that a commercially available hydrophilic polytetrafluoroethylene (PTFE) membrane can be used as a separator to significantly extend the cycling life of Zn anodes. Compared with traditional brittle GF separators, the wetted PTFE membrane shows higher mechanical strength (a stress of 34.3 MPa at 41.4% strain) (Fig. 9o) and good hydrophilicity (Fig. 9r), both of which help suppress the growth of Zn dendrites. It was found that the uniform and robust porous structure of the membrane promotes even Zn^{2+} distribution and achieves a high Zn^{2+} transference number (0.81), which ensures stable and reversible Zn plating/stripping.

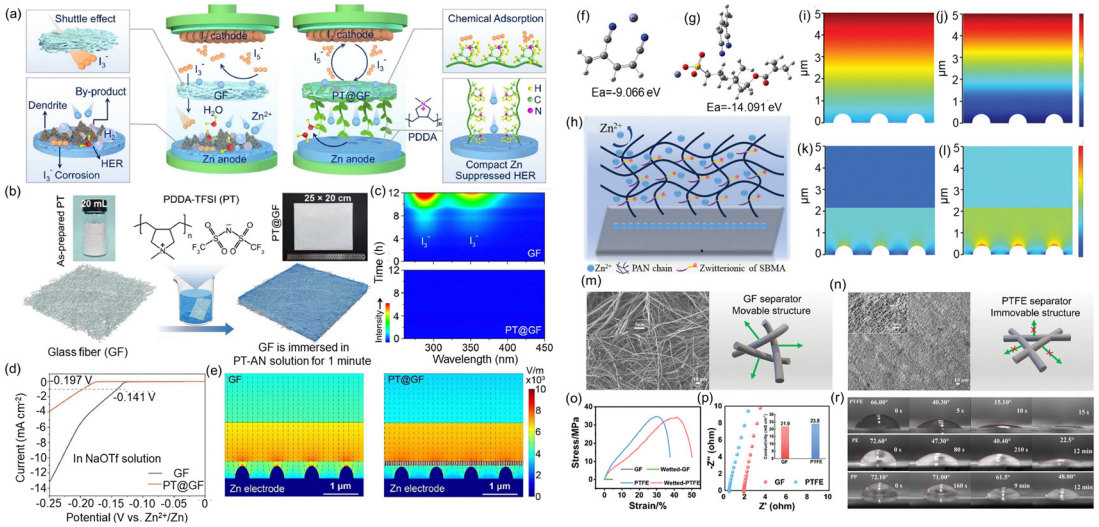

Fig. 9 (a) Schematic representation of Zn–I_2 batteries assembled with commercial GF and PT@GF separators. (b) Diagram depicting the preparation process of the PT@GF separator, with inset images showing the as-prepared PT powder (left) and the large-scale PT@GF separator (right). (c) UV-Vis spectra of 1 mM I_3^- solutions with GF and PT@GF soaking at various time intervals. (d) LSV curves for Zn‖Ti cells using GF and PT@GF separators with NaOTf aqueous solution. (e) Simulations illustrating the electric field distribution on Zn electrodes with GF and PT@GF separators during Zn^{2+} plating. Reproduced with permission.[121] Copyright 2025, Elsevier. (f) and (g) DFT models showing Zn^{2+} binding with PAN and PAN@SBMA. (h) Schematic of Zn^{2+} plating behavior through the PAN@SBMA separator. (i) and (j) Zn^{2+} concentration distribution in cells with PAN@SBMA and PAN separators. (k) and (l) Electric field distribution in cells with PAN@SBMA and PAN separators. Reproduced with permission.[122] Copyright 2024, Wiley-VCH. (m) and (n) SEM images and schematic structures of GF and PTFE separators. (o) Stress–strain curves of GF and PTFE. (p) Ionic conductivity of GF and PTFE separators. (r) Contact angles of PTFE, PE, and PP separators. Reproduced with permission.[123] Copyright 2024, Wiley-VCH.

5.2 COF-based separators

The framework of covalent organic frameworks (COFs) is built from various organic linkers. COFs combine porosity with structural precision, multifunctionality, and tunability, making them an excellent platform for designing materials with targeted properties. COFs uniquely combine high porosity with structural precision, versatility, and tunability, making them an excellent platform for designing controllable materials with targeted properties.

To simultaneously address critical issues like Zn dendrite growth and electrolyte-cathode interface instability, Xu *et al.*[124] proposed a quasi-single-ion conductive separator based on COFs. This separator uses Zn^{2+}-substituted COF-$SO_3Zn_{0.5}$ (referred to as COF-Zn), where the abundant sulfonate groups provide efficient Zn^{2+} conductivity (Fig. 10a). The researchers employed bacterial cellulose (BC) as a binder, physically mixing it with COF-Zn and preparing a thin and flexible separator *via* a simple filtration process. This separator not only exhibits quasi-single-ion conductivity but also selectively promotes Zn^{2+} migration, effectively suppressing dendrite growth. The COF-Zn separator, only 25 μm thick, combined with BC's good hydrophilicity, allows the battery to operate stably with as little as 20 μL mg^{-1} of electrolyte, reducing cathode dissolution and improving energy density. Experiments showed that the Zn‖Zn symmetrical batteries with COF-Zn separators cycled for over 2900 hours at 0.2 mA cm^{-2}, demonstrating extremely high stability (Fig. 10b).

5.3 Nafion-based separators

Nafion is a cation-exchange membrane known for its excellent ion selectivity, thanks to its sulfonic acid groups. It is widely used as a separator in flow batteries and, due to its flexibility and good electrochemical properties, is also commonly employed as a solid-state electrolyte. Ghosh *et al.*[125] prepared a Zn^{2+}-doped Nafion ionomer membrane (3 M-Nafion) *via* an electrochemical deposition method (Fig. 11a). In this membrane, Zn^{2+} coordinate with the $-SO_3^-$ groups, enhancing both the Zn^{2+} transference number and the overall ionic conductivity. Additionally, the 3 M-Nafion membrane exhibits lower activation energy, smaller Zn plating/stripping voltage gaps, more uniform Zn^{2+} deposition, and effective suppression of dendrite growth.

Notably, Nafion membranes not only regulate the Zn plating/stripping behavior at the anode but also significantly influence the interaction between certain cathode materials and the electrolyte. Wu *et al.*[126] developed a Zn–Nafion composite membrane by exchanging Na^+ with Zn^{2+}. This membrane helps create a uniform electric field at the Zn anode and reduces concentration gradients in the electrolyte, effectively suppressing dendrite formation (Fig. 11b). Moreover, the strong affinity between the Zn–Nafion membrane and the cathode material enhances proton (H^+) participation during H^+/Zn^{2+} co-insertion reactions while minimizing side reactions. The membrane also facilitates the transformation of the by-product $Zn_4SO_4(OH)_4{\cdot}nH_2O$ into a dense solid protective layer, preventing the dissolution of cathode active materials. As a result, the battery shows improved energy density and capacity retention. After 150 cycles, the battery using the Zn–Nafion membrane retains 85.7% of its capacity, compared to just 44.8% with a conventional separator. Importantly, the Zn–Nafion membrane is also reusable, making it economically advantageous.

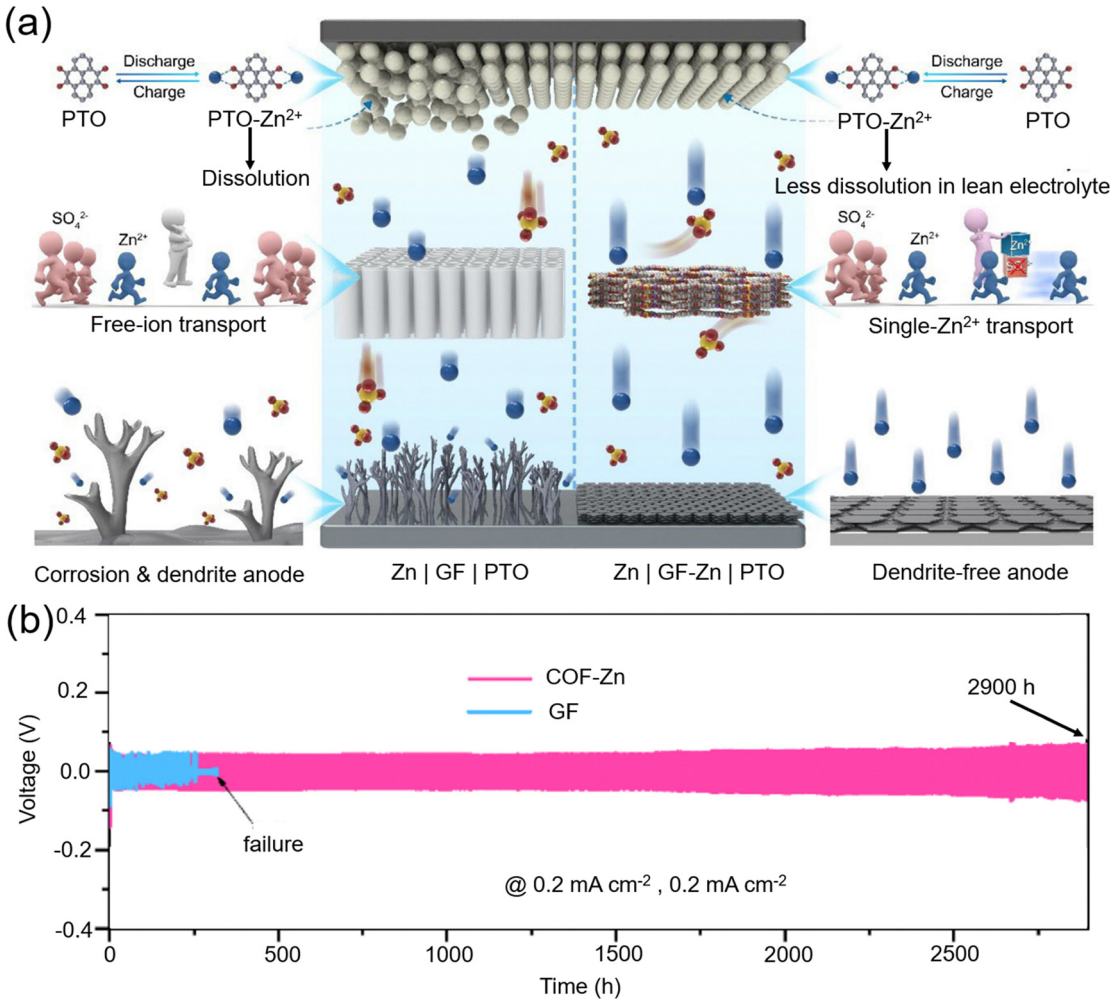

Fig. 10 (a) Diagram showing small-molecule-based Zn‖PTO batteries with different separators. (b) Cycling performance comparison for COF-Zn and GF separators. Reproduced with permission.[124] Copyright 2025, Wiley-VCH.

To further enhance membrane performance, some researchers have introduced multifunctional groups into the Nafion structure to increase ion transport pathways and add new functionalities such as improved wettability and stronger Zn^{2+} affinity. Yuan *et al.*[127] fabricated a lignin@Nafion composite membrane by integrating lignin into Nafion (Fig. 11c and d). Rich in $-SO_3^-$ groups, the composite membrane strongly coordinates with Zn^{2+}, reconstructing ion transport channels and guiding Zn^{2+} to deposit preferentially on the (002) crystal plane. This suppresses the vertical growth of Zn sulfate by-products (ZHS), thereby preventing short circuits. The presence of lignin also increases ion transport, improves conductivity, reduces cost, and promotes lateral distribution of by-products along the electrode surface while favoring Zn deposition on the (100) crystal plane (Fig. 11e). Under the same conditions, batteries with lignin@Nafion separators deliver 1.2 times the capacity of conventional batteries.

In summary, Nafion membranes help achieve uniform Zn^{2+} transport, regulate electrolyte pH, and prevent the dissolution of cathode materials, thereby improving battery cycling stability. However, the high cost and limited economic efficiency of Nafion remain barriers to its widespread commercialization. Future research should focus on improving sustainability and reducing costs to support its broader application in energy storage systems.

5.4 Cellulose-based separators

Cellulose-based separators have shown great potential in the modification of AZBs, as demonstrated by their widespread application across various battery systems. In recent years, significant progress has been made in using cellulose-related materials to expand the application scope of AZBs. As a polymer composed of repeating units, cellulose offers several outstanding properties, including environmental friendliness, recyclability, low cost for large-scale production, strong resistance to swelling, and the ability to introduce functional groups through molecular design. These advantages have made cellulose-based separators a subject of growing interest and extensive research in the field of AZBs.

Yang *et al.*[128] developed a multifunctional separator composed of nanocellulose coated with *in situ* hydrolyzed Zr^{4+} species (Zr-CNF). Due to the crosslinking effect of Zr^{4+} and its

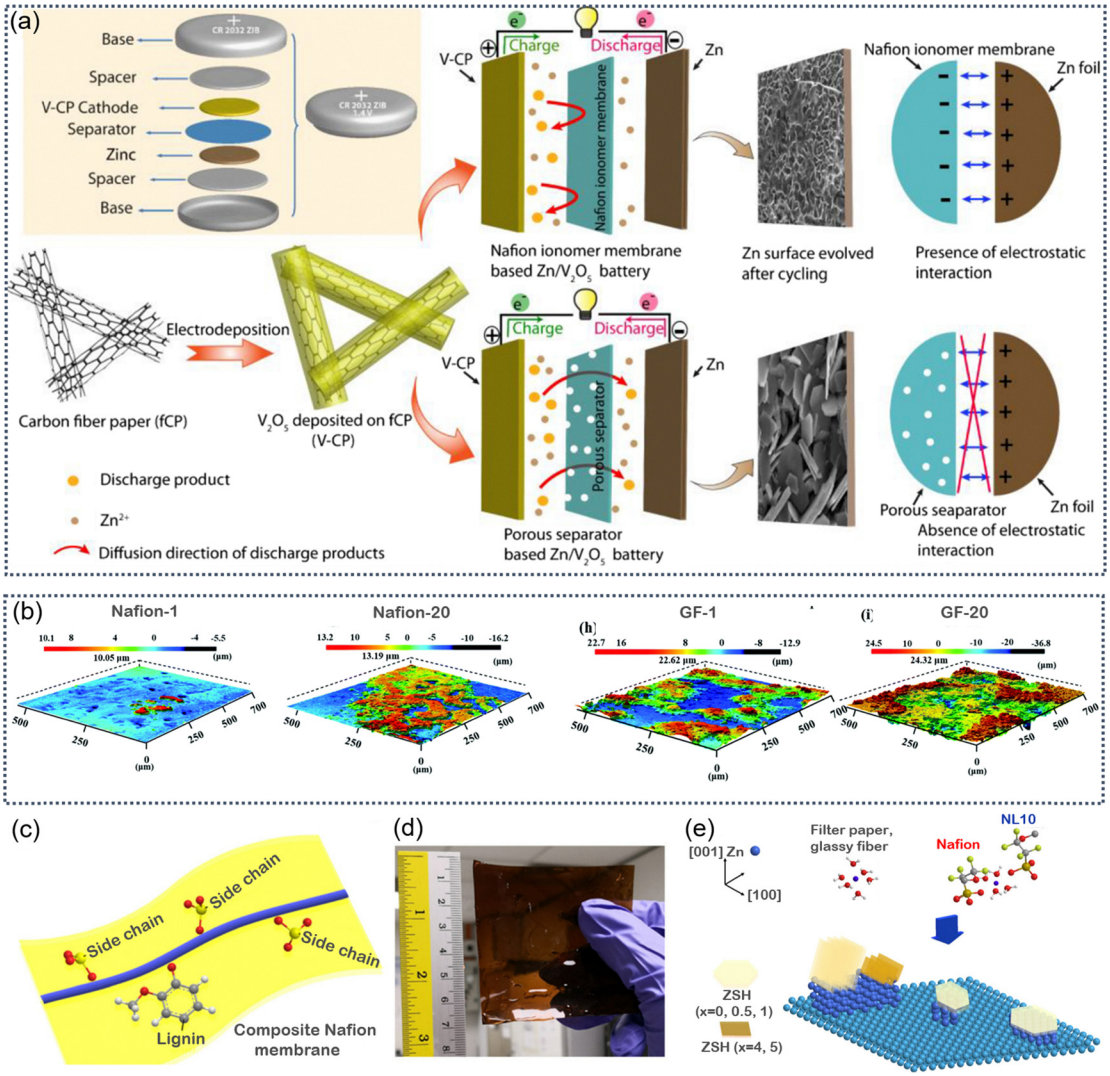

Fig. 11 (a) Diagram showing different Zn/V_2O_5 cell setups with Zn^{2+}-integrated Nafion ionomer and a regular porous membrane separator. Reproduced with permission.[125] Copyright 2019, Wiley-VCH. (b) 3D surface images of Zn–Nafion and GF separators after the 1st cycle and 20th cycle. Reproduced with permission.[126] Copyright 2021, Royal Society of Chemistry. (c) Design diagram of composite biomass waste lignin@Nafion membranes. (d) Photo of a 7 × 7 cm lignin@Nafion membrane. (e) Illustration showing how the membranes affect the Zn metal surface. The interaction between SO_3^- groups in Nafion and Zn^{2+} changes Zn^{2+} coordination from its form in the electrolyte, leading to different growth patterns of Zn deposits and ZHS byproducts. Reproduced with permission.[127] Copyright 2019, Wiley-VCH.

ability to disrupt hydrogen bonding in cellulose through hydrolysis, the resulting separator exhibited excellent anti-swelling properties and stable porous structure. The Zr-CNF material was synthesized using a straightforward ion-coordination and hydrolysis-precipitation method (Fig. 12a).

During battery operation, the separator maintained uniform Zn^{2+} ion flux, high ionic conductivity, and a favorable Zn^{2+} transference number. In addition, the amorphous Zr–O coating on the surface induced a uniform directional electric field around the separator *via* Maxwell–Wagner polarization. This promoted faster Zn^{2+} ion transport, reduced the nucleation overpotential, and facilitated uniform Zn deposition. As a result, the anti-swelling Zr-CNF separator effectively stabilized the Zn anode. The battery using this separator demonstrated a long cycle life of over 1600 hours with a stable and flat voltage plateau, indicating excellent Zn plating/stripping performance (Fig. 12b). Moreover, CE tests revealed that the cell with a traditional TCNF separator short-circuited after only 250 cycles, while the cell with the Zr-CNF separator maintained stable cycling for over 450 cycles with an impressive average CE of 99.7% (Fig. 12c).

Yang *et al.*[129] developed a low-cost and multifunctional fly ash/cellulose composite separator (FACNF) using a simple solution-casting method. Fig. 12d schematically illustrates the fabrication process of the cost-effective FACNF separator. Recycled fly ash microspheres and cellulose nanofiber dispersion were mixed in deionized water, cast onto a glass substrate, and then dehydrated overnight. As shown in the digital photograph (Fig. 12d), the resulting FACNF separator has a large area of 22 cm × 14 cm. The prepared separator was found to

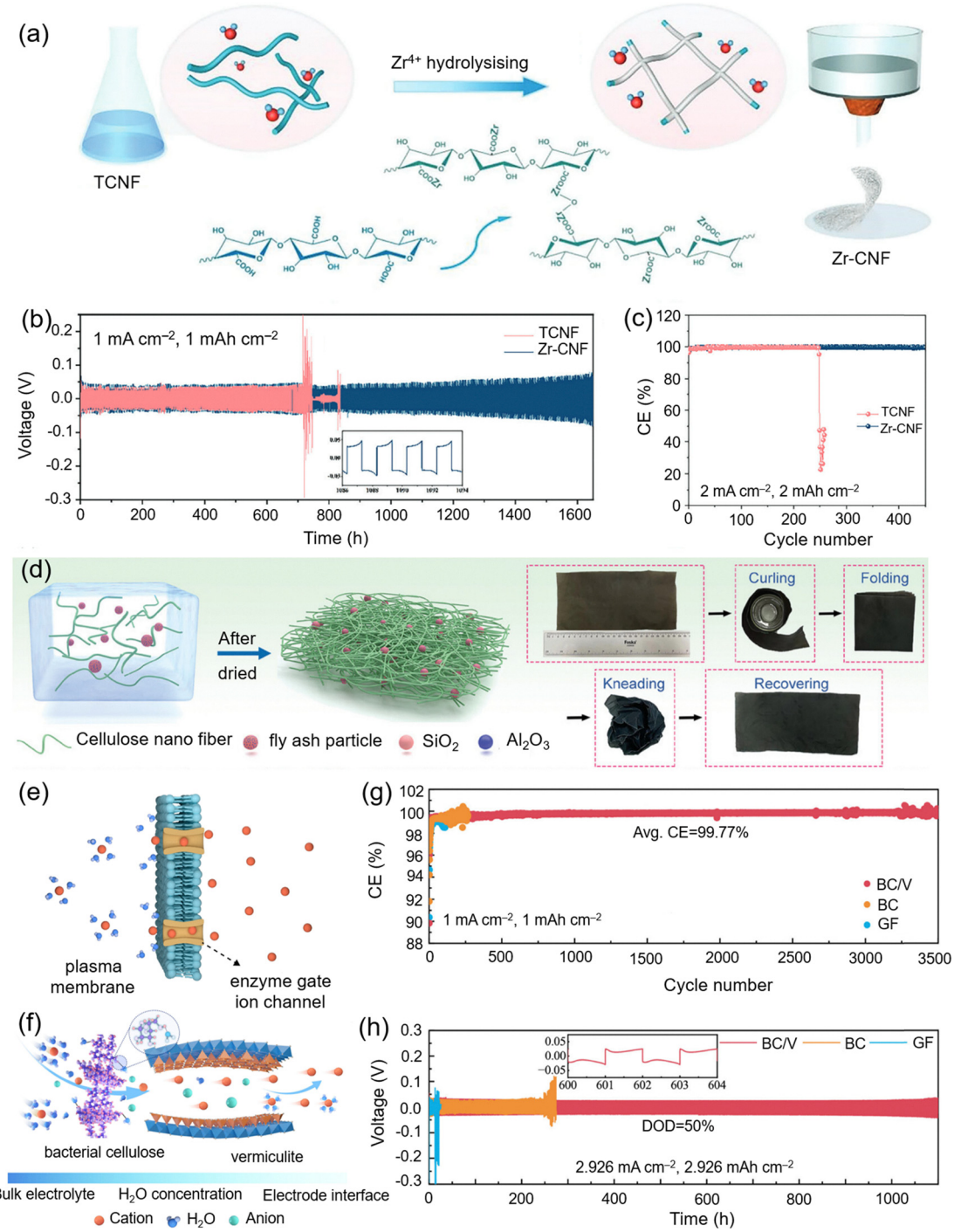

Fig. 12 (a) Diagram showing how the Zr-CNF separator is made. (b) Cycling performance of different Zn‖Zn symmetric cells at 1 mA cm^{-2} and 1 mAh cm^{-2}. (c) Voltage curves of Zn‖Cu half cells with Zr-CNF separator at 2 mA cm^{-2} and 2 mAh cm^{-2}. Reproduced with permission.[128] Copyright 2023, Wiley-VCH. (d) Process for making FACNF separators. (e) Photos of FACNF separators in different states: curling, folding, kneading, and recovering. Reproduced with permission.[129] Copyright 2024, Wiley-VCH. (f) Illustration of how the plasma membrane controls selective ion flow. (g) Illustration showing how the BC/V separator controls ion and solvent transport in water-based electrolytes. (h) Coulombic efficiency of Zn‖Cu asymmetric cells at 1 mA cm^{-2} and 1 mAh cm^{-2}. (i) Cycling stability of Zn|Zn cells at 2.926 mA cm^{-2} and 2.926 mAh cm^{-2} (50% depth of discharge). Reproduced with permission.[130] Copyright 2025, Elsevier.

promote uniform Zn deposition along the (002) crystal plane, enabling long-term cycling stability of the Zn anode. Experimental results showed that the addition of fly ash improved ionic conductivity (5.76 mS cm^{-1}), lowered the energy barrier for hydrated Zn^{2+} desolvation, and suppressed hydrogen evolution and surface corrosion on the Zn anode. Moreover, theoretical calculations revealed that, compared to Zn(100) and Zn(101) crystal planes, fly ash particles exhibit a lower chemical

binding energy with the Zn(002) surface. This preferential interaction promotes the deposition of Zn along the (002) orientation, thereby effectively mitigating the formation and growth of Zn dendrites.

Li *et al.*[130] developed a lightweight and mechanically strong separator made from bacterial cellulose and vermiculite. As shown in Fig. 12e and f, this highly flexible membrane helps selective ion transport through enzyme-controlled ion channels. The separator works through a combined effect, improving the selective movement of Zn^{2+} and speeding up desolvation, while trapping active water molecules inside its structure. These features help Zn^{2+} spread evenly and create a stable, low-water environment at the electrode surface. Because of this, the separator allows the Zn anode to last over 7000 hours (3500 cycles) with an average Coulombic efficiency of 99.77% (Fig. 12g). In Zn‖Zn cells with 50% depth of discharge, the BC/V separator kept stable cycling for more than 1100 hours (550 cycles), maintaining a nucleation overpotential below 10 mV (Fig. 12h).

6. Large-scale separator production

Given the application of AZBs in grid-scale energy storage, the development of scalable and efficient separator fabrication methods is of critical importance. To address this, Wang *et al.*[131] designed a dendrite-resistant separator using a simple and scalable hot-pressing strategy (Fig. 13a). In this approach, a mixture of metal–organic framework (MOF) precursors—including metal salts, organic ligands, and a fluxing agent—is uniformly distributed onto a nonwoven fiber matrix, followed by a 30-minute hot-pressing step. During this process, MOF crystals form *in situ via* coordination reactions, coating the fiber surface uniformly. These MOF structures provide abundant

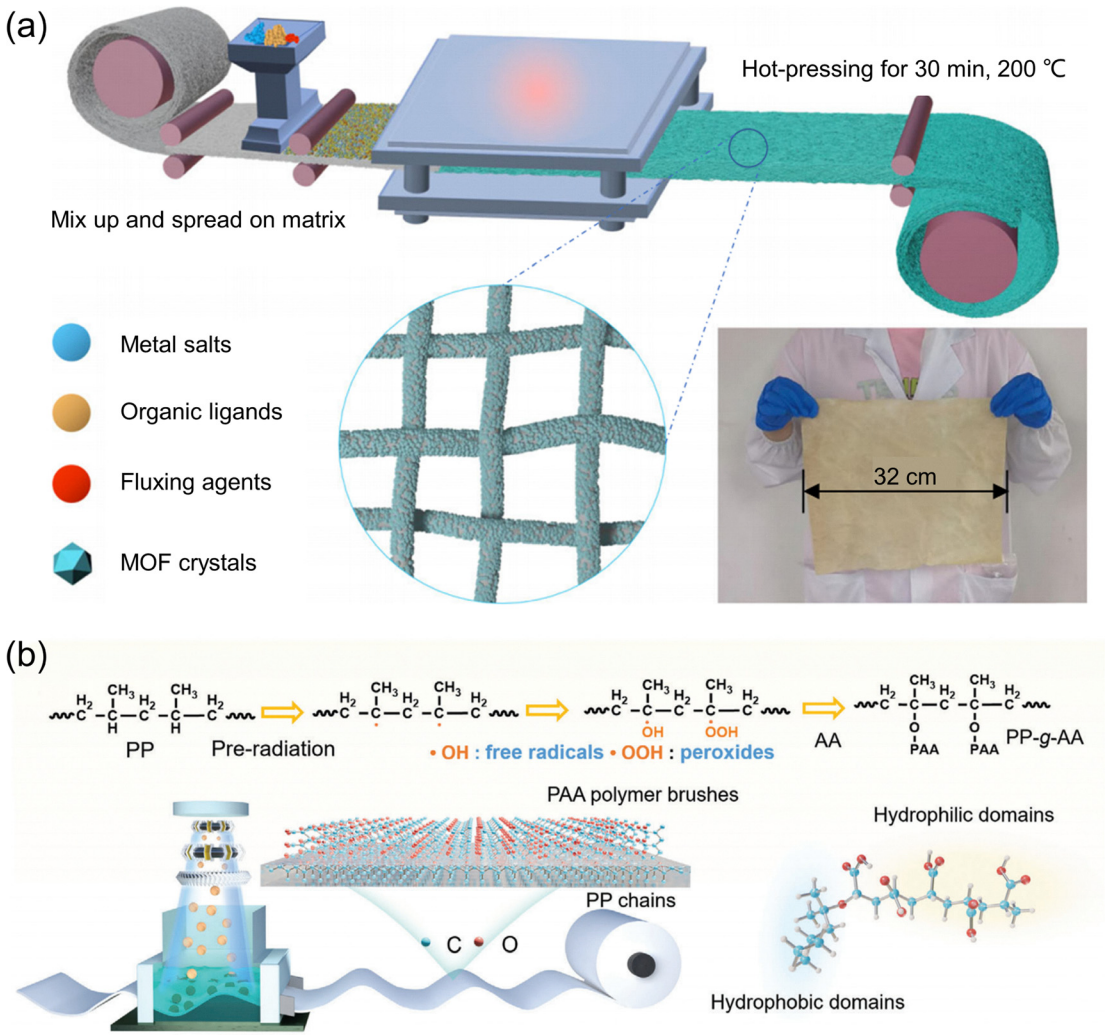

Fig. 13 (a) Fabrication process of HTS using a one-step hot-press strategy, resulting in a Zn-based HTS product. Reproduced with permission.[131] Copyright 2025, Springer Nature. (b) Schematic representation of the preparation method for the PP-*g*-AA separator. Reproduced with permission.[133] Copyright 2024, Wiley-VCH.

nitrogen-containing functional groups and a high specific surface area (190.8 $m^2 g^{-1}$), which enhance Zn^{2+} adsorption and facilitate efficient ion transport. The resulting hot-pressed separator (HTS) demonstrates both excellent electrochemical performance and strong potential for large-scale manufacturing. To further validate its scalability, a wide-area HTS membrane (32 cm × 28 cm) was successfully fabricated using this one-step process, highlighting its promise for practical grid-scale applications.

Zhu *et al.*[132] developed a hydrophilic, radiation-grafted polypropylene (PP) separator with a thickness of only 25 μm, suitable for large-scale production at rates reaching millions of square meters per day. As shown in Fig. 13b, the fabrication process begins with electron beam (E-beam) pre-irradiation of a porous PP separator, generating peroxide (•OOH) and hydroxyl (•OH) radicals. The activated PP matrix is then immersed in an acrylic acid (AA) monomer solution of varying concentrations, initiating a grafting reaction to form a polyacrylic acid-modified separator. Subsequent ultrasonication removes unreacted monomers and homopolymers. The resulting PP-*g*-AA membrane features a dual-domain structure: a hydrophobic PP backbone that effectively resists water intrusion and suppresses parasitic reactions, and hydrophilic polyacrylic acid grafts that act as dynamic Zn^{2+} transport pathways. This architecture enables precise modulation of interfacial electric fields and Zn^{2+} concentration gradients, facilitating uniform Zn^{2+} flux and dendrite-free Zn deposition.

7. Summary and outlook

AZBs have emerged as promising candidates for grid-scale energy storage because of their safety, cost-effectiveness, and high theoretical capacity. However, challenges such as Zn dendrite, HER, anode corrosion, and cathode material dissolution limit their widespread use. The separator plays a key role in regulating ion transport, reducing side reactions, and improving Zn deposition uniformity. Recent advancements in separator materials and modification strategies show great potential in overcoming these challenges.

This review systematically categorizes separator modifications based on their location—anode side, cathode side, and full-separator modifications—and discusses key strategies such as ion-selective layers, interfacial engineering, and composite functional membranes. These modifications have been shown to improve Zn^{2+} flux regulation, suppress dendrite growth, and enhance long-term cycling stability. Emerging materials like COFs, MOFs, and inorganic–organic hybrid separators have also been highlighted for their potential in optimizing battery performance.

The review provides a comprehensive analysis of the mechanisms underlying these modifications, offering theoretical insights and design principles for the development of next-generation AZB separators. It also emphasizes the importance of balancing various performance parameters, such as porosity, mechanical strength, and chemical stability, to achieve optimal separator performance.

However, existing separators still face challenges in ion selectivity, dendrite suppression, interface stability, and cost control, limiting the battery's lifespan and energy density. In the future, separator design should focus on thinness, high ion selectivity, enhanced interface stability, improved corrosion resistance, and low-cost scalable manufacturing to further enhance the overall performance of AZBs.

7.1 Key factors for future separator design

Future separator design should focus on several key factors to meet the demands of high-performance AZBs. First, ion selectivity and transport regulation are essential, requiring high Zn^{2+} conductivity while effectively blocking anions or undesired species such as polyiodides. Second, to mitigate dendrite formation, separators must help homogenize the electric field and ion flux. Third, chemical and electrochemical stability in mildly acidic or neutral electrolytes is crucial to prevent degradation and ensure long-term performance. Additionally, mechanical strength and flexibility are needed to withstand volume changes and mechanical stress during cycling. Finally, the materials and fabrication methods should offer scalability and cost-effectiveness to facilitate large-scale commercial application.

7.2 Major practical challenges

Future separator development also faces several critical challenges. Ensuring compatibility with high-loading electrodes is essential, as many laboratory-scale separators struggle to maintain performance under practical conditions. Long-term durability is another concern, as functional coatings may degrade or delaminate during extended cycling. Additionally, the complexity of functionalization, such as multilayer or hybrid structures, can introduce manufacturing difficulties and reproducibility issues. Lastly, there are inherent trade-offs between key properties—for example, improving ion selectivity may reduce ionic conductivity—making it difficult to achieve an optimally balanced separator design.

7.3 Lightweight design to increase energy density

The thickness of the separator directly affects the battery's volumetric energy density and ion transport resistance. Commercialized AZBs typically use GF or polyolefin separators, but these separators are relatively thick (>30 μm), which hinders Zn^{2+} transport and reduces the battery's energy density. Therefore, future efforts should focus on developing thinner separators with a thickness of less than 20 μm while ensuring mechanical strength and electrochemical stability. For instance, nanocellulose separators, ultra-thin composite-coated separators, or interface-enhanced layered structures could be employed to reduce thickness while maintaining high ion transport capabilities. Indeed, while reducing separator thickness is a proven strategy to enhance the gravimetric and volumetric energy density of AZBs, it introduces mechanical integrity, puncture resistance, and dimensional stability that must be carefully considered for practical applications, especially in large-format, flexible, or high-power systems.

7.4 High ion selectivity to improve Zn^{2+} transport efficiency

Current separators exhibit poor selectivity between Zn^{2+} and other anions, leading to increased side reactions and shortened battery life. In the future, single-ion conductors or gradient ion distribution separators should be developed to regulate Zn^{2+} migration pathways through chemical modification. For example, separator materials based on COFs and MOFs scan provide highly ordered Zn^{2+} transport channels, improving ion screening ability. Additionally, a gradient Zn^{2+} concentration control strategy could be used to form a Zn^{2+}-rich region at the anode and a Zn^{2+}-deficient region at the cathode, optimizing Zn^{2+} deposition behavior and enhancing battery stability.

7.5 Enhanced interface stability to suppress dendrite growth

The formation of Zn dendrites is one of the most significant issues during the operation of AZBs, leading to separator puncture, short circuits, and capacity degradation. Therefore, future separators should have the ability to regulate interfaces, stabilizing Zn^{2+} deposition and reducing dendrite growth. For example:

• functional layer modification: coating the separator surface with oxides (ZnO, CuO), two-dimensional materials (MXene, g-C_3N_4), or polymer coatings can evenly distribute Zn^{2+} nucleation sites and improve the reversibility of plating/stripping.

• Asymmetric separator design: a functional layer that anchors Zn^{2+}, such as $BaTiO_3$ nanoparticles or nitrogen-containing functional groups, can be constructed on the side near the Zn anode, promoting uniform deposition and reducing the risk of local Zn^{2+} oversaturation.

7.6 Improved corrosion resistance and hydrogen evolution suppression

The HER takes place during the charging and discharging processes, resulting in the depletion of the electrolyte and the corrosion of the Zn anode. Future strategies could involve modifying the separator with amphiphilic molecules, fluorinated polymer coatings, or superhydrophobic/hydrophilic interface designs to optimize separator performance. For example:

• hydrophilic–hydrophobic gradient separators: maintaining hydrophobicity near the Zn anode side to reduce water infiltration, while enhancing hydrophilicity at the electrode/electrolyte interface to promote uniform Zn^{2+} distribution.

7.7 Low-cost and large-scale manufacturing

The commercialization of future AZBs requires separators with low cost and scalable manufacturing capabilities. For example:

• Spray-curing technology: this method can quickly fabricate large-area functionalized separators, improving production efficiency.

• Radiation-grafted polymerization: high-selectivity functional separators can be continuously fabricated on industrial production lines.

• Hot-press compositing: a simple hot-pressing process can be used to manufacture nanocoated separators, reducing preparation costs and improving mechanical strength.

The future development of AZB separators requires continuous optimization in terms of thinness, ion selectivity, interface stability, corrosion resistance, and cost control. Through rational material design and advanced manufacturing processes, the battery's cycle life, rate performance, and energy density can be significantly enhanced, providing more reliable solutions for grid-scale energy storage and high-power applications in AZBs.

Conflicts of interest

The authors declare no conflict of interest.

Data availability

This review does not include any primary research results, software, or code, nor does it involve the generation or analysis of new data.

Acknowledgements

C. Z. acknowledges the support from the National Key R&D Program of China under Project 2019YFA0705104, the grants from the Research Grants Council of the Hong Kong Special Administrative Region, China (Project No. R5019-22, Project No. CityU PDFS2122-1S05, and Project No. CityU 11214023), the Talent Recruitment Project of Guangdong Province (no. 2019QN01C883), the Shenzhen Science and Technology Innovation Project (JCYJ20220818102402004) and HIT-CityU Joint Laboratory on Zinc-based Batteries. H. L. acknowledges the support from the Shenzhen Science, Technology and Innovation Commission Basic Research Project (Grant No. JCYJ20240813153125033).

References

1 A. Chel and G. Kaushik, *Alexandria Eng. J.*, 2018, **57**, 655–669.
2 P. A. Østergaard, N. Duic, Y. Noorollahi and S. Kalogirou, *Renewable Energy*, 2022, **199**, 1145–1152.
3 P. A. Østergaard, N. Duic, Y. Noorollahi, H. Mikulcic and S. Kalogirou, *Renewable Energy*, 2020, **146**, 2430–2437.
4 S. Tabrizian, *Sustainable Dev.*, 2019, **27**, 537–544.
5 M. Yavari and I. M. Bohreghi, *Appl. Energy*, 2025, **377**, 124654.
6 C. Cao, Y. Zhong and Z. Shao, *Chin. J. Chem.*, 2023, **41**, 1119–1141.
7 H. Cavers, P. Molaiyan, M. Abdollahifar, U. Lassi and A. Kwade, *Adv. Energy Mater.*, 2022, **12**, 2200147.
8 R. Gond, W. van Ekeren, R. Mogensen, A. J. Naylor and R. Younesi, *Mater. Horiz.*, 2021, **8**, 2913–2928.
9 S. Hosamane, N. Kottam and A. Chalil Suresh, *Wiley Interdiscip. Rev.: Energy Environ.*, 2025, **14**, e544.
10 Y. K. Liu, C. Z. Zhao, J. Du, X. Q. Zhang, A. B. Chen and Q. Zhang, *Small*, 2023, **19**, e2205315.
11 H. Lv, X. Chu, Y. Zhang, Q. Liu, F. Wu and D. Mu, *Mater. Today*, 2024, **78**, 181–208.

12 R. Tao, Y. Gu, Z. Du, X. Lyu and J. Li, *Nat. Rev. Clean Technol.*, 2025, **1**, 116–131.
13 X. Tian, Y. Yi, B. Fang, P. Yang, T. Wang, P. Liu, L. Qu, M. Li and S. Zhang, *Chem. Mater.*, 2020, **32**, 9821–9848.
14 T. Zhou, R. Huang, Q. Lu, P. Liu, L. Hu, K. Zhang, P. Bai, R. Xu, X. Cao, Z. Sun, S. Duan, R. Liu, Y. Qin, X. Sun, Y. Zhang, Y. Li, Y. Yan, M. Liu and X. Wang, *Energy Storage Mater.*, 2024, **72**, 103689.
15 P. Li, H. Kim, J. Ming, H.-G. Jung, I. Belharouak and Y.-K. Sun, *eScience*, 2021, **1**, 3–12.
16 Y. Zheng, Y. Shen, J. Guo, J. Li, J. Wang, D. Ning, Y. Liu, Y. Huang, Y. Tang, Y. Deng, H. Yan and H. Shao, *Nano Res. Energy*, 2024, **3**, e9120118.
17 J. J. Roy, D. M. Phuong, V. Verma, R. Chaudhary, M. Carboni, D. Meyer, B. Cao and M. Srinivasan, *Carbon Energy*, 2024, **6**, e492.
18 Y. Wan, B. Huang, W. Liu, D. Chao, Y. Wang and W. Li, *Adv. Mater.*, 2024, **36**, e2404574.
19 S. Gao, Z. Zhu, H. Fang, K. Feng, J. Zhong, M. Hou, Y. Guo, F. Li, W. Zhang, Z. Ma and F. Li, *Adv. Mater.*, 2024, **36**, e2311523.
20 B. Zhong, C. Liu, D. Xiong, J. Cai, J. Li, D. Li, Z. Cao, B. Song, W. Deng, H. Peng, H. Hou, G. Zou and X. Ji, *ACS Nano*, 2024, **18**, 16468–16488.
21 S. Li, Y. Shang, X. Ren, A. Zhao, N. Chen, L. Li, F. Wu and R. Chen, *ACS Nano*, 2025, **19**, 16584–16596.
22 A. Zhou, J. Zhang, M. Chen, X. Li, S. Li, J. Ma, T. Lv, X. Zhu, G. Feng and L. Suo, *J. Am. Chem. Soc.*, 2025, **147**, 11811–11820.
23 U. Ali, B. Liu, H. Jia, Y. Li, Y. Li, Y. Hao, L. Zhang, S. Xing, L. Li and C. Wang, *Small*, 2024, **20**, e2305866.
24 L. Li, S. Jia, Y. Shi, C. Wang, H. Qiu, Y. Ji, M. Cao and D. Zhang, *Inorg. Chem. Front.*, 2024, **11**, 2246–2259.
25 Y. N. Liu, J. L. Yang, Z. Y. Gu, X. Y. Zhang, Y. Liu, M. Y. Su, X. L. Zhang, I. V. Zatovsky, K. Li, J. M. Cao and X. L. Wu, *Angew. Chem., Int. Ed.*, 2024, **63**, e202316925.
26 R. Wang, S. Zhang, S. Peng, Y. Tong and X. Hu, *Carbon Neutrality*, 2024, **3**, 6.
27 H. Wu, J. Hao, Y. Jiang, Y. Jiao, J. Liu, X. Xu, K. Davey, C. Wang and S. Z. Qiao, *Nat. Commun.*, 2024, **15**, 575.
28 M. Xia, J. Zhou and B. Lu, *Adv. Energy Mater.*, 2025, **15**, 2404032.
29 F. Dong, B. Yang, X. Zhang, Z. Yang, S. Wang, Z. Hou and P. Chen, *ACS Appl. Mater. Interfaces*, 2025, **17**, 1332–1340.
30 Q. Guo, S. Han, Y. Lu, R. Xiao, J. Li, Q. Hao, X. Rong, S. Weng, Y. Niu, F. Ding, Y. Yang, H. Xia, X. Wang, F. Xie, L. Zhou, X. Hou, H. Li, X. Huang, L. Chen and Y. S. Hu, *Nat. Commun.*, 2025, **16**, 4707.
31 I. Jeong, S. Kim, Y. Kim, C. Kim, J. Kang, J. H. Ha, Y. Cho, S. J. Kang, J. Ryu, J. W. Han and S. Park, *Adv. Mater.*, 2025, **37**, e2412652.
32 G. Fang, J. Zhou, A. Pan and S. Liang, *ACS Energy Lett.*, 2018, **3**, 2480–2501.
33 Y. H. Lee, Y. Jeoun, J. H. Kim, J. Shim, K. S. Ahn, S. H. Yu and Y. E. Sung, *Adv. Funct. Mater.*, 2024, **34**, 2310884.
34 Y. Lv, Y. Xiao, L. Ma, C. Zhi and S. Chen, *Adv. Mater.*, 2022, **34**, e2106409.
35 X. Shi, J. Xie, J. Wang, S. Xie, Z. Yang and X. Lu, *Nat. Commun.*, 2024, **15**, 302.
36 J. Wei, P. Zhang, J. Sun, Y. Liu, F. Li, H. Xu, R. Ye, Z. Tie, L. Sun and Z. Jin, *Chem. Soc. Rev.*, 2024, **53**, 10335–10369.
37 T. Wu, C. Hu, Q. Zhang, Z. Yang, G. Jin, Y. Li, Y. Tang, H. Li and H. Wang, *Adv. Funct. Mater.*, 2024, **34**, 2315716.
38 J. Zhu, Z. Tie, S. Bi and Z. Niu, *Angew. Chem., Int. Ed.*, 2024, **63**, e202403712.
39 Y. Shen, P. Fu, J. Liu, K. Sun, H. Wen, P. Liu, H. Lv, T. Gu, X. Yang and L. Chen, *Nano Res. Energy*, 2024, **3**, e9120115.
40 J. Li, A. Azizi, S. Zhou, S. Liu, C. Han, Z. Chang, A. Pan and G. Cao, *eScience*, 2025, **5**, DOI: **10.1016/j.esci.2024.100294**.
41 L. Deng, X. Xie, W. Song, A. Pan, G. Cao, S. Liang and G. Fang, *Chem. Eng. J.*, 2024, **488**, 151104.
42 Q. Dong, Q. Nian, X. Luo, J. Fan, J. Jiang, Z. Cui, D. Ruan and X. Ren, *Sci. China: Chem.*, 2024, **68**, 526–535.
43 X. Luo, Q. Nian, Q. Dong, D. Ruan, Z. Cui, Z. Wang, B. Q. Xiong and X. Ren, *Adv. Energy Mater.*, 2025, **15**, 2403187.
44 Q. Nian, X. Luo, D. Ruan, Y. Li, B. Q. Xiong, Z. Cui, Z. Wang, Q. Dong, J. Fan, J. Jiang, J. Ma, Z. Ma, D. Wang and X. Ren, *Nat. Commun.*, 2024, **15**, 4303.
45 X. Yang, Z. Dong, G. Weng, Y. Su, J. Huang, H. Chai, Y. Zhang, K. Wu, J. B. Baek, J. Sun, D. Chao, H. Liu, S. Dou and C. Wu, *Adv. Energy Mater.*, 2024, **14**, 2401293.
46 W. Zhang, W. Qi, K. Yang, Y. Hu, F. Jiang, W. Liu, L. Du, Z. Yan and J. Sun, *Energy Storage Mater.*, 2024, **71**, 103616.
47 W. Du, E. H. Ang, Y. Yang, Y. Zhang, M. Ye and C. C. Li, *Energy Environ. Sci.*, 2020, **13**, 3330–3360.
48 J. Hao, X. Li, X. Zeng, D. Li, J. Mao and Z. Guo, *Energy Environ. Sci.*, 2020, **13**, 3917–3949.
49 B. Li, X. Zhang, T. Wang, Z. He, B. Lu, S. Liang and J. Zhou, *Nanomicro Lett*, 2021, **14**, 6.
50 A. Naveed, A. Ali, T. Rasheed, X. Wang, P. Ye, X. Li, Y. Zhou, S. Mingru and Y. Liu, *J. Power Sources*, 2022, **525**, 231122.
51 R. Qin, Y. Wang, L. Yao, L. Yang, Q. Zhao, S. Ding, L. Liu and F. Pan, *Nano Energy*, 2022, **98**, 107333.
52 J. Zheng, Z. Huang, F. Ming, Y. Zeng, B. Wei, Q. Jiang, Z. Qi, Z. Wang and H. Liang, *Small*, 2022, **18**, e2200006.
53 C. Zhu, P. Li, G. Xu, H. Cheng and G. Gao, *Coord. Chem. Rev.*, 2023, **485**, 215142.
54 A. Xia, X. Pu, Y. Tao, H. Liu and Y. Wang, *Appl. Surf. Sci.*, 2019, **481**, 852–859.
55 Y. Zeng, X. Zhang, R. Qin, X. Liu, P. Fang, D. Zheng, Y. Tong and X. Lu, *Adv. Mater.*, 2019, **31**, e1903675.
56 Y. Guo, C. Liu, L. Xu, K. Huang, H. Wu, W. Cai and Y. Zhang, *Energy Mater.*, 2022, **2**, 200032.
57 Y. Li, Y.-F. Guo, Z.-X. Li, P.-F. Wang, Y. Xie and T.-F. Yi, *Energy Storage Mater.*, 2024, **67**, 103300.
58 C. Mao, Y. Chang, X. Zhao, X. Dong, Y. Geng, N. Zhang, L. Dai, X. Wu, L. Wang and Z. He, *J. Energy Chem.*, 2022, **75**, 135–153.
59 C. Choi, J. B. Park, J. H. Park, S. Yu and D.-W. Kim, *Chem. Eng. J.*, 2023, **456**, 141015.
60 X. Hu, J. Borowiec, Y. Zhu, X. Liu, R. Wu, A. M. Ganose, I. P. Parkin and B. D. Boruah, *Small*, 2024, **20**, e2306827.

61 G.-Q. Liu, B. Fu, Z.-X. Liu, L.-Y. Li, S.-Q. Liang and G.-Z. Fang, *Rare Met.*, 2024, **43**, 5005–5016.
62 Y. Meng, M. Wang, J. Xu, K. Xu, K. Zhang, Z. Xie, Z. Zhu, W. Wang, P. Gao, X. Li and W. Chen, *Angew. Chem., Int. Ed.*, 2023, **62**, e202308454.
63 H. Zhang, G. Zhu, J. Lu, Y. Hou, Y. Bao, P. Liu and Y. Zhang, *Small*, 2025, **21**, 2408848.
64 P. Xue, C. Guo, W. Gong, Y. Chen, X. Chen, X. Li, J. Yang, Q. Zhang, K. Davey, K. Zhu, J. Mao and Z. Guo, *Angew. Chem., Int. Ed.*, 2025, **64**, e202500295.
65 B. Li, K. Yang, J. Ma, P. Shi, L. Chen, C. Chen, X. Hong, X. Cheng, M. C. Tang, Y. B. He and F. Kang, *Angew. Chem., Int. Ed.*, 2022, **61**, e202212587.
66 Y. Chai, X. Xie, Z. He, G. Guo, P. Wang, Z. Xing, B. Lu, S. Liang, Y. Tang and J. Zhou, *Chem. Sci.*, 2022, **13**, 11656–11665.
67 Y. Du, Y. Feng, R. Li, Z. Peng, X. Yao, S. Duan, S. Liu, S. C. Jun, J. Zhu, L. Dai, Q. Yang, L. Wang and Z. He, *Small*, 2024, **20**, e2307848.
68 X. Zheng, Z. Liu, J. Sun, R. Luo, K. Xu, M. Si, J. Kang, Y. Yuan, S. Liu, T. Ahmad, T. Jiang, N. Chen, M. Wang, Y. Xu, M. Chuai, Z. Zhu, Q. Peng, Y. Meng, K. Zhang, W. Wang and W. Chen, *Nat. Commun.*, 2023, **14**, 76.
69 M. Zhou, C. Fu, L. Qin, Q. Ran, S. Guo, G. Fang, X. Lang, Q. Jiang and S. Liang, *Energy Storage Mater.*, 2022, **52**, 161–168.
70 Q. Ma, W. Song, X. Zhang, N. Yang, B. Wu, C. Zheng, M. Fujishige, K. Takeuchi, M. Endo, J. Niu and F. Wang, *Adv. Funct. Mater.*, 2025, **35**, 2422159.
71 J. Cao, Y. Jin, H. Wu, Y. Yue, D. Zhang, D. Luo, L. Zhang, J. Qin and X. Yang, *Adv. Energy Mater.*, 2025, **15**, 2403175.
72 Y. Ding, X. Zhang, T. Wang, B. Lu, Z. Zeng, Y. Tang, J. Zhou and S. Liang, *Energy Storage Mater.*, 2023, **62**, 102949.
73 Z. Hu, F. Zhang, Y. Zhao, H. Wang, Y. Huang, F. Wu, R. Chen and L. Li, *Adv. Mater.*, 2022, **34**, e2203104.
74 S. Wang, S. Wang, Z. Wei, Y. Wang, D. Zhang, Z. Chen and C. Zhi, *Nat. Commun.*, 2025, **16**, 1800.
75 L. Cao, D. Li, E. Hu, J. Xu, T. Deng, L. Ma, Y. Wang, X. Q. Yang and C. Wang, *J. Am. Chem. Soc.*, 2020, **142**, 21404–21409.
76 F. Wang, O. Borodin, T. Gao, X. Fan, W. Sun, F. Han, A. Faraone, J. A. Dura, K. Xu and C. Wang, *Nat. Mater.*, 2018, **17**, 543–549.
77 P. Chen, X. Lin, B. Yang, Y. Gao, Y. Xiao, L. Li, H. Zhang, L. Li, Z. Zheng, J. Wang and S. Chou, *Adv. Funct. Mater.*, 2024, **34**, 2409368.
78 J. Chen, M. Chen, H. Ma, W. Zhou and X. Xu, *Energy Rev.*, 2022, **1**, 100005.
79 B. Li, Y. Zeng, W. Zhang, B. Lu, Q. Yang, J. Zhou and Z. He, *Sci. Bull.*, 2024, **69**, 688–703.
80 L. Li, S. Jia, Z. Cheng and C. Zhang, *ChemSusChem*, 2023, **16**, e202202330.
81 Y. Qin, P. Liu, Q. Zhang, Q. Wang, D. Sun, Y. Tang, Y. Ren and H. Wang, *Small*, 2020, **16**, 2003106.
82 M.-Y. Wang, R.-B. Huang, J.-F. Xiong, J.-H. Tian, J.-F. Li and Z.-Q. Tian, *Acta Phys.-Chim. Sin.*, 2024, **40**, 2307017.
83 Y. Zong, H. He, Y. Wang, M. Wu, X. Ren, Z. Bai, N. Wang, X. Ning and S. X. Dou, *Adv. Energy Mater.*, 2023, **13**, 2300403.
84 H. Zhou, J. Gu, Y. Wei, W. Zhang, J. Kang, J.-Q. Huang, B. Zhang, C. Hu and X. Lin, *J. Power Sources*, 2023, **558**, 232649.
85 L. Li, M. Sun, B. Hao, W. Chen, C. Zhu, L. Zhang, X. Shen, X. Zhou, J. Zhou, C. Yan, X. Liu and T. Qian, *J. Phys. Chem. Lett.*, 2024, **15**, 380–390.
86 R. Fazaeli, H. Aliyan, Z. Huang, Y. Wang and Y. Li, *ACS Omega*, 2025, **10**, 3228–3261.
87 J. Zhu, M. Yanilmaz, K. Fu, C. Chen, Y. Lu, Y. Ge, D. Kim and X. Zhang, *J. Membr. Sci.*, 2016, **504**, 89–96.
88 C. Xu, B. Li, H. Du and F. Kang, *Angew. Chem., Int. Ed.*, 2012, **51**, 933–935.
89 M. H. Alfaruqi, V. Mathew, J. Gim, S. Kim, J. Song, J. P. Baboo, S. H. Choi and J. Kim, *Chem. Mater.*, 2015, **27**, 3609–3620.
90 L. Kang, M. Cui, F. Jiang, Y. Gao, H. Luo, J. Liu, W. Liang and C. Zhi, *Adv. Energy Mater.*, 2018, **8**, 1801090.
91 Q. Zhao, W. Huang, Z. Luo, L. Liu, Y. Lu, Y. Li, L. Li, J. Hu, H. Ma and J. Chen, *Sci. Adv.*, 2018, **4**, eaao1761.
92 N. Zhang, F. Cheng, Y. Liu, Q. Zhao, K. Lei, C. Chen, X. Liu and J. Chen, *J. Am. Chem. Soc.*, 2016, **138**, 12894–12901.
93 F. Wu, F. Du, P. Ruan, G. Cai, Y. Chen, X. Yin, L. Ma, R. Yin, W. Shi, W. Liu, J. Zhou and X. Cao, *J. Mater. Chem. A*, 2023, **11**, 11254–11263.
94 S. Liu, Q. Han, C. He, Z. Xu, P. Huang, L. Cai, H. Chen, H. Zheng, Y. Zhou, M. Wang, H. Tian, W. Q. Han and H. Ying, *ACS Nano*, 2024, **18**, 25880–25892.
95 C. Li, Z. Sun, T. Yang, L. Yu, N. Wei, Z. Tian, J. Cai, J. Lv, Y. Shao, M. H. Rummeli, J. Sun and Z. Liu, *Adv. Mater.*, 2020, **32**, e2003425.
96 Y. Su, B. Liu, Q. Zhang, J. Peng, C. Wei, S. Li, W. Li, Z. Xue, X. Yang and J. Sun, *Adv. Funct. Mater.*, 2022, **32**, 2204306.
97 P. Jiang, Q. Du, C. Lei, C. Xu, T. Liu, X. He and X. Liang, *Chem. Sci.*, 2024, **15**, 3357–3364.
98 Y. Wang, X. Jin, J. Xiong, Q. Zhu, Q. Li, R. Wang, J. Li, Y. Fan, Y. Zhao and X. Sun, *Adv. Mater.*, 2024, **36**, e2404093.
99 L. Zhang, J. Huang, H. Guo, L. Ge, Z. Tian, M. Zhang, J. Wang, G. He, T. Liu, J. Hofkens, D. J. L. Brett and F. Lai, *Adv. Energy Mater.*, 2023, **13**, 2203790.
100 Y. Zhao, X. Chen, W. Guo and C. Zha, *Carbon Neutralization*, 2024, **3**, 918–949.
101 H. Bi, D. Tian, Z. Zhao, Q. Yang, Y. Yuan, R. Zhang, L. Ai, X. Wang and J. Qiu, *Adv. Funct. Mater.*, 2025, **35**, 2423115.
102 J. Yang, Q. Dai, S. Hou, C. Han and L. Zhao, *Adv. Mater.*, 2025, **37**, 2418258.
103 Y. Kang, G. Chen, H. Hua, M. Zhang, J. Yang, P. Lin, H. Yang, Z. Lv, Q. Wu, J. Zhao and Y. Yang, *Angew. Chem., Int. Ed.*, 2023, **62**, e202300418.
104 F. Bu, Z. Sun, W. Zhou, Y. Zhang, Y. Chen, B. Ma, X. Liu, P. Liang, C. Zhong, R. Zhao, H. Li, L. Wang, T. Zhang, B. Wang, Z. Zhao, J. Zhang, W. Li, Y. S. Ibrahim, Y. Hassan, A. Elzatahry, D. Chao and D. Zhao, *J. Am. Chem. Soc.*, 2023, **145**, 24284–24293.

105 Y. Tan, D. Chen, T. Yao, Y. Zhang, C. Miao, H. Yang, Y. Wang, L. Li, V. Kotsiubynskyi, W. Han and L. Shen, *Adv. Sci.*, 2024, **11**, e2407410.
106 Y. Song, P. Ruan, C. Mao, Y. Chang, L. Wang, L. Dai, P. Zhou, B. Lu, J. Zhou and Z. He, *Nano Micro. Lett.*, 2022, **14**, 218.
107 P. Yang, K. Zhang, S. Liu, W. Zhuang, Z. Shao, K. Zhu, L. Lin, G. Guo, W. Wang, Q. Zhang and Y. Yao, *Adv. Funct. Mater.*, 2024, **34**, 2410712.
108 H. Ma, J. Yu, M. Chen, X. Han, J. Chen, B. Liu and S. Shi, *Adv. Funct. Mater.*, 2023, **33**, 2307384.
109 P. Tian, Y. Gao, S. Huang, Y. Cao, Z. Liu, Y. Huo, M. Li, X. Gu and L. Wu, *Adv. Energy Mater.*, 2024, **14**, 2401830.
110 Y. Liang, D. Ma, N. Zhao, Y. Wang, M. Yang, J. Ruan, G. Yang, H. Mi, C. He and P. Zhang, *Adv. Funct. Mater.*, 2022, **32**, 2112936.
111 Z. Zhao, Y. Zhang, H. Zhang, X. Shi, H. Zhao, J. Liu, J. Liu and L. Li, *Nano Lett.*, 2025, **25**, 7483–7490.
112 Y. Kang, G. Chen, H. Hua, M. Zhang, J. Yang, P. Lin, H. Yang, Z. Lv, Q. Wu and J. Zhao, *Angew. Chem., Int. Ed.*, 2023, **62**, e202300418.
113 L. Deng, K. Sun, J. Liu, Z. Li, J. Cao and S. Liao, *Molecules*, 2024, **29**, 3147.
114 Z. Sun, J. Zhang, X. Jiao and Z. Li, Modified Separator with Biomass-Derived Carbon for Dendrite-Free and Boosting Cycling Stability of Zinc-Ion Battery, Available at SSRN: DOI: **10.2139/ssrn.4879884**.
115 B. Wu, P. Wang, H. Yang, Y. Liang, W. Ni, G. Xu, X. Wei and L. Yang, *J. Power Sources*, 2023, **580**, 233323.
116 Q. Zhang, L. Wan, X. Gao, S. Cheng, N. Gao, C. J. Carmalt, Y. Dai, G. He and H. Li, *ACS Appl. Mater. Interfaces*, 2024, **16**, 69388–69397.
117 F. Ma, K. Xie, S. Wu, C. Zhang, X. Liao and Q. Wang, *Batteries*, 2023, **9**, 387.
118 Q. Gou, H. Luo, L. Qu, F. Yu, K. Wang, S. Zhang, Z. Luogu, B. Zhang, Y. Zheng and B. Song, *J. Energy Chem.*, 2025, **101**, 191–200.
119 H. Zhang, H. Yang, B. Wu, Y. Liang, W. Ni, G. Xu and L. Yang, *Ionics*, 2024, **30**, 237–246.
120 B. Cao, Q. Qu, B. Jiang, T. Zou, S. Zhen, P. Wang, K. Li, J. Zhang, H. Guo and T. Zhang, *J. Mater. Chem. A*, 2024, **12**, 31185–31194.
121 W. Yuan, X. Qu, Y. Wang, X. Li, X. Ru, D. Jia, L. Zhao, Y. Hou, J. Shen, Z. Shen and N. Zhang, *Energy Storage Mater.*, 2025, **76**, 104130.
122 L. Cheng, W. Li, M. Li, S. Zhou, J. Yang, W. Ren, L. Chen, Y. Huang, S. Yu and J. Wei, *Adv. Funct. Mater.*, 2024, **34**, 2408863.
123 G. Wu, R. Zhu, W. Yang, Y. Yang, J. Okagaki, Z. Lu, J. Sun, H. Yang and E. Yoo, *Adv. Funct. Mater.*, 2024, **34**, 2316619.
124 J. Xu, Y. Yang, Q. Dai, Z. Zheng, Y. Cao, Y. Cheng, B. Peng, L. Ma and Y. Wang, *Angew. Chem., Int. Ed.*, 2025, **64**, e202423118.
125 M. Ghosh, V. Vijayakumar and S. Kurungot, *Energy Technol.*, 2019, **7**, 1900442.
126 B. Wu, Y. Wu, Z. Lu, J. Zhang, N. Han, Y. Wang, X.-M. Li, M. Lin and L. Zeng, *J. Mater. Chem. A*, 2021, **9**, 4734–4743.
127 D. Yuan, W. Manalastas, Jr., L. Zhang, J. J. Chan, S. Meng, Y. Chen and M. Srinivasan, *ChemSusChem*, 2019, **12**, 4889–4900.
128 S. Yang, Y. Zhang, Y. Zhang, J. Deng, N. Chen, S. Xie, Y. Ma and Z. Wang, *Adv. Funct. Mater.*, 2023, **33**, 2304280.
129 C. Yang, P. Woottapanit, Y. Yue, S. Geng, J. Cao, X. Zhang, G. He and J. Qin, *Small*, 2024, **20**, e2311203.
130 T. Li, Y. Gong, H. Yang, Y. Liu, X. Dong, Y. Xu, H. Ma, C. Wei, S. Zhang, F. Huang, M. Yang and T. Lin, *Energy Storage Mater.*, 2025, **79**, 104311.
131 D. Wang, S. Hu, T. Li, C. Chang, S. Li, S. Guo, H. Li, Q. Liu, J. Gong, J. Zhou and C. Han, *Nat. Commun.*, 2025, **16**, 259.
132 X. Zhu, Z. Xu, T. Zhang, J. Zhang, Y. Guo, M. Shan, K. Wang, T. Shi, G. Cui and F. Wang, *Adv. Funct. Mater.*, 2024, **34**, 2407262.
133 X. Zhu, Z. Xu, T. Zhang, J. Zhang, Y. Guo, M. Shan, K. Wang, T. Shi, G. Cui, F. Wang, G. Xu and M. Zhu, *Adv. Funct. Mater.*, 2024, **34**, 2407262.